UNIVERSIDADE DE SÃO PAULO
Instituto de Física de São Carlos

Paulina Rossi Ferreira

Comparative characterization of Upper-Pleistocene and modern day coral skeleton

São Carlos
2023

Paulina Rossi Ferreira

Comparative characterization of Upper-Pleistocene and modern day coral skeletons

Dissertation presented to the Graduate Program in Physics at the Instituto de Física de São Carlos, Universidade de São Paulo to obtain the degree of Master of Science.

Concentration area: Biomolecular Physics

Advisor: Prof. Dr. Antônio Carlos Hernandes

Corrected Version
(Original version available on the Program Unit)

São Carlos
2023

Ferreira, Paulina Rossi
Comparative characterization of Upper-Pleistocene and modern day coral skeleton / Paulina Rossi Ferreira; advisor Antonio Carlos Hernandes - corrected version -- São Carlos 2023.
78 p.

Dissertation (Master's degree - Graduate Program in Biomolecular Physics) -- Instituto de Física de São Carlos, Universidade de São Paulo - Brasil , 2023.

1. Aragonite. 2. Physical properties. 3. Scleractinian corals. I. Hernandes, Antonio Carlos, advisor. II. Title.

AGRADECIMENTOS

Primeiro, agradeço a minha mãe, sem a qual eu não teria seguido nenhum dos meus sonhos e cá estou aqui vivendo-o. Você é minha luz, minha pastora e minha pedra fundamental, eu te amo.

Ao meu orientador, obrigada pela oportunidade e pela confiança em mim, tanto em 2014 quanto em 2020, para trabalhar contigo. Renovou minha paixão pela Ciência e abriu meus olhos para todo um novo campo que jamais pensei em alcançar.

Ao meu amor, sem você eu não teria feito metade do trabalho e teria chorado o dobro. A sua existência é extremamente preciosa.

A todos os meus amigos, a quem amo incondicionalmente. Vocês me ouviram desabafar e duvidar de mim mesma e reclamar e chorar, mas sempre tiveram um momento para me lembrar de que eu sou capaz. Espero também poder ser o farol de vocês na tempestade.

Aos meus colegas de bancada, agradeço pela paciência, eu sei que dei trabalho a vários de vocês. Desejo a todos o melhor.

Este estudo foi em parte financiado pela Coordenação de Aperfeiçoamento de Pessoal de Nível Superior - Brasil (CAPES) - Código Financeiro 001.

ACKNOWLEDGEMENTS

I want to first thank my mother, without whom I wouldn't have pursued any dreams and here I am, living it. You are my light, my shepherd and my rock, I love you.

I want to thank my advisor for the opportunity and for the trust in me, both in 2014 and now in 2020, to work with him. It renewed my passion in Science and opened my eyes to a whole new field that I never thought myself in, and I am loving every moment of it.

To my love, without you I am sure I would not have completed half of the work and would have cried double the times. Thank you, you are a very precious existence.

To all my friends, whom I love unconditionally. You all heard me vent and doubt myself and complain and cry, but always took a moment to remind me that I could do it. I hope I can also be the lighthouse through your storms.

To my research colleagues, thank you for all the patience, I know I gave a lot of you a hard time. Wish you all the best.

This study was financed in part by the Coordenação de Aperfeiçoamento de Pessoal de Nível Superior - Brasil (CAPES) - Finance Code 001.

ABSTRACT

FERREIRA, P. R. **Comparative characterization of Upper-Pleistocene and modern day Coral skeletons.** 2023.78p. Dissertation (Master of Science) – Instituto de Física de São Carlos, Universidade de São Paulo, São Carlos, 2023.

Reefs are marine formations with biological, ecological and scientific value, such as harboring enormous biodiversity, protecting the shoreline from waves and marking sea-level and sea temperature evolution through epochs. Corals thrive in a variety of habitats according to their adaptations, having colonized depths from 0 to 2000 m from the sea surface and all latitudes across Earth. Reefs are mainly constituted by scleractinian corals, also known as stony corals, that synthesize a calcareous skeleton which act as scaffold for other organisms to shelter. The synthesized limestone captures carbon and performs an important role in Oceans' carbon cycle as carbon sinks. Since the decade of 1950, scleractinian corals are known for depositing aragonite which is a metastable calcium carbonate polymorph with rare natural occurrence, being calcite the most stable polymorph. Coral aragonite have shown interesting physical properties such as distorted aragonite unit cells and different phase transition temperatures when compared to geological aragonite, also notable mechanical strength capable of enduring oceanic tides. This work studies two colonial corals found in brazilian fauna for their age, chemical composition, crystalline structure and thermal behavior. Assessed specimens are *Mussismilia hispida* (Verrill, 1901) collected at 10 m deep and *Lophelia pertusa* (Linnaeus, 1758) collected 852 m deep, called *Mh* and *Lp* respectively. Results from radiocarbon dating tell that *Mh* is 22 years old modern coral and *Lp* is 12000 years old fossilized Pleistocene corals. Both samples are composed of aragonite and present trace elements originated in seawater, such as Mg, Na, Sr, S and Cl. Their thermal behavior and phase transition temperatures were proven to be distinct from other scleractinian corals previously studied. Although all corals presented the beginning of phase transition at 285 ºC, our samples ended the process 310 ºC, 100 ºC cooler than the model corals, around 400 ºC. This phenomenon is reputed to corals being of different clades, hence having a fundamental genetic difference, but this has to be studied further.

Keywords: Aragonite. Physical properties. Scleractinian corals.

RESUMO

FERREIRA, P. R. **Caracterização comparativa de esqueletos de corais do Pleistoceno Superior e moderno.** 2023. 78p. Dissertação (Mestre em Ciência) – Instituto de Física de São Carlos, 2023.

Recifes de corais são formações marinhas de alto valor biológico, ecológico e científico, dado suas diversas funções, como abarcar enorme biodiversidade, proteger a linha costeira de ondas e marcar a evolução do nível do mar e da temperatura da superfície do mar através das épocas. Corais prosperam em uma gama de habitats de acordo com sua adaptação, tendo colonizado profundidades de 0 a 2000 m abaixo do nível do mar e todas as latitudes pela Terra. Recifes são principalmente formados por corais escleractínios, conhecidos como corais rochosos, que sintetizam um esqueleto calcário que atua como abrigo para outros organismos. Este calcário sintetizado captura carbono e tem participação importante no ciclo do carbono oceânico, atuando como capturadores de carbono. Desde a década 1950, sabe-se que corais escleractínios depositam aragonita, que é um polimorfo metaestável de carbonato de cálcio, sendo calcita o polimorfo mais estável. Aragonita coralínea mostrou propriedades físicas interessantes como célula unitária distorcida e temperaturas de transição de fase diferentes quando comparadas com aragonita de origem geológica, além de propriedades mecânicas notáveis dada a capacidade de persistir em correntes oceânicas. Este trabalho estudou de dois corais coloniais encontrados na fauna brasileira a suas idades, composições químicas, estruturas cristalinas e comportamento térmico. Os dois espécimes são *Mussismilia hispida* (Verrill, 1901) coletado a 10 m de profundidade e *Lophelia pertusa* (Linnaeus, 1758) coletado a 852 m de profundidade, chamados aqui de *Mh* e *Lp*. Resultados de datação de radiocarbono contam que *Mh* tem 22 anos e é um coral moderno e *Lp* tem 12000 anos de idade e é um coral fossilizado do Pleistoceno. Ambas as amostras são compostas de aragonita e apresentam elementos traço originados da água do mar, como Mg, Na, Sr, S and Cl. O comportamento térmico e temperaturas de transições de fase foram provadas de serem distintas às de outros corais escleractínios estudados. Embora todos os corais apresentem início de transição de fase a 285 ºC, nossas amostras finalizaram o processo a 310 ºC, 100 ºC abaixo da temperatura dos modelos, 400 ºC. Este fenômeno é reputado aos corais serem de clados diferentes, portanto possuem diferenças genéticas fundamentais, mas ainda deve ser estudado mais profundamente.

Palavras-chave: Aragonita. Propriedades físicas. Corais escleractíneos.

LIST OF FIGURES

Figure 1 - Schematic view of polyp with labeled structures. 23

Figure 2 - Phase diagram of calcium carbonate polymorphs formation. 25

Figure 3 - a) In blue, thermogravimetric (TG) measurement in which mass is continuously measured in increasing temperature, assessing for disintegration of coral aragonite sample from *Pavona sp*. Thermal decomposition of CaCO3 is expected to begin at 650 oC (823 K). TG is coupled with mass chromatography that separates released compounds by atomic mass, shown in green and pink curves. Green curve indicates release of water vapor, pink curve indicates release of CO2; b) powder X-ray diffractometry for increasing temperatures, between 300 and 700 oC. Diffractograms show the progression of phase transition from aragonite to calcite. Phase transition is completed at 450 oC (723 K). 28

Figure 4 - Starting and ending temperatures of phase transition for aragonite to calcite for materials of different origins. Coral, *Galaxea fascicularis* highlighted in red. 29

Figure 5 - SEM images of Porites coral skeleton surface, a) rod-like and acicular cements divided in primary aragonite (PA), secondary aragonite (SA) and chipped surface from the cutting process for a 400 year-old coral sample, SA surface is marked by a spiculed surface made of aragonite needles; b) magnified region of SA in a), evidence of acicular aragonite formation; c) acicular SA found in surface of 350 year-old coral sample with more densely packed needles; d) SA needles on a skeletal dissepiment (D) which separates layers of growth; e) frontier between PA and SA divided by dissepiment, SA is present below dissepiment while PA is above. 32

Figure 6 - Discrimination of growth regions between rapid accretion deposit and thickening deposit on coral skeleton. 34

Figure 7 - a) Illustration of *L. pertusa* specimen. Starting in (b) all images are progressive enlargements of interesting sections; b) photograph of cut L. pertusa fragment; c) micrograph of interest area in L.pertusa branch; d) Reflected light image of RAD and TD. Opaque (O) and translucent (T) bands are indicated. To the right, an EBSD shows the crystal growth based on direction indicated by color: blue is [001], red is [010] and green is [100]. 35

Figure 8 - Micro-computed tomography (μCT) scans of transplanted *S. pistillata* corals A) in a longitudinal cut and B) in transversal cut 0.5 mm from coral tip. Yellow arrows indicate thicker skeletal formations of corals from 60 m depth both originated and transplanted. Analysis shows that internal divisions of skeleton, septa, are more evenly formed in deeper waters along with thicker external walls in opposition to non-uniform septa and thinner walls in shallow water. 36

Figure 9 - Map of collection sites per sample according to coordinates. 40

Figure 10 - Photograph of a) *Mussismilia hispida*, b) two fragments of *Lophelia pertusa.* 41

Figure 11 - Example of calibration curve graph for interpreting radiocarbon years in calendar years. 44

Figure 12 - a) Position of each fragment within branches of *Lophelia pertusa* specimen. Illustration made by the author; b) Photographs of live *Lophelia pertusa* polyps in different life stages. 49

Figure 13 - a) Mh sample with cut location; b) transversal section of *Mh*. 50

Figure 14 - X-ray diffractograms measured for both species, peaks normalized to 100. 52

Figure 15 - measured X-ray diffractograms and refined patterns from Rietveld method. a) *Mh* and b) *Lp*. 53

Figure 16 - 3D models of aragonite primitive cell. Calcium in blue, carbonates highlighted with gray planes. 54

Figure 17 - a) Rietveld refined synchrotron radiation diffractogram of coral sample *Favia sp*; d) Rietveld refined synchrotron radiation diffractogram of geological aragonite. Peaks (102) and (200) shown in inset; c) and d) peaks (102) and (200) for *Mh* and *Lp*. 55

Figure 18 - SEM images of different coral species with different growth fronts and skeletal organizations. 57

Figure 19 - SEM images of a) and b) non-treated sample; c) and d) 200 oC thermally-treated sample; e) and f) 200 oC thermally-treated. 59

Figure 20 - SEM images of spiculated surfaces: a) sample treated at 200 oC, white encircled area reference zoomed region in b); c) sample treated at 260 oC, below the phase transition temperature, d) is a zoomed region of c). 60

Figure 21 - SEM images of fragment *Lp*B, a) non-treated sample showing cut surface to reveal flattened needles and small grains in skeletal growth scar; b) zoomed region of a) shows fan-like formations of

aragonite stemming from a calcification center; c) sample treated at 260 oC, showing porous region with preserved microstructure; d) zoomed region of c), in which is visible mature skeleton, highlighted by red arrows. Mature skeleton is organized in a fan of flattened needles. 61

Figure 22 - Chemically etched *Mussismilia hispida* subsamples for a) 30 min, b) 60 min. 62

Figure 23 - SEM image of *Lp* surface. Emphasis on mature skeleton displayed by fan of flat aragonite needles and center or calcification, alternatively RAD, marked by asterisk. 63

Figure 24 - Two step TG analysis for a) *Mh*, b) *Lp*. 64

Figure 25 - Compared step 1 TG for *Mh* and *Lp*. 65

Figure 26 - X-ray diffractograms for varied temperatures, a) *Mh* and b) *Lp*. Diffectograms tell the sample's crystalline structure at selected temperatures to show the progression of phase transition: at 260 oC sample is still aragonite, at 285 oC sample has a fraction of both aragonite and calcite, at 400 oC sample has fully transformed into calcite. 67

LIST OF TABLES

Table 1 - Taxonomic classification of stony corals. 21
Table 2 - Lattice parameters for aragonite and calcite of variable origins. 26
Table 3 - Site collection, condition of samples and preservation method. 39
Table 4 - 14C quantification and dating. 47
Table 5 - Samples macroscopic characteristics. 48
Table 6 - EDS results for each sample. 50
Table 8 - Rietveld refinement results according to reference. 55
Table 9 - GSAS II Rietveld refinement result report for samples treated at 285 oC. 66

LIST OF ABBREVIATIONS AND ACRONYMS

CENA/USP	Centro de Energia Nuclear na Agricultura da Universidade de São Paulo
Dp	*Desmophyllum pertusum*
ECF	Extracellular calcifying fluid
EDS	Electron Dispersive Spectroscopy
Fs	*Favia stelata*
Lp	*Lophelia pertusa*
Mh	*Mussismilia hispida*
SEM	Scanning Electron Microscopy
XRD	X - ray diffraction

SUMMARY

1	**INTRODUCTION**	**19**
2	**LITERATURE REVIEW**	**21**
2.1	**Overview on corals**	**21**
2.2	**Structure and material properties of geological calcium carbonate**	**24**
2.3	**Biogenic materials analysis**	**26**
2.3.1	**Structure and properties**	**26**
2.3.2	**Coral growth mechanisms and adaptation**	**33**
2.4	**Summary**	**37**
3	**SAMPLES AND METHODOLOGY**	**39**
3.1	**Sample collection and description**	**39**
3.1.1	**Mussismilia hispida (Verrill, 1901)**	**40**
3.1.2	**Lophelia pertusa (Linnaeus, 1758)**	**40**
3.2	**Sample preparation**	**41**
3.3	**Energy Dispersive Spectroscopy and Scanning Electron Microscopy**	**42**
3.4	**Radiocarbon dating**	**43**
3.5	**Thermogravimetric analysis**	**44**
3.6	**X-Ray powder diffraction**	**45**
4	**RESULTS AND DISCUSSION**	**47**
4.1	**Carbon dating**	**47**
4.2	**Samples at eye level**	**48**
4.3	**Chemical composition**	**50**
4.4	**Crystal structure**	**51**
4.5	**SEM analysis**	**56**
4.6	**Thermal behavior**	**63**
5	**CONCLUSIONS**	**69**
5.1	**Project limitations**	**69**
5.2	**Future directions**	**70**
REFERENCES		**71**

1 INTRODUCTION

Materials science investigates the relation between structure of matter and physical properties that it presents. Structure, in a materials sciences context, refers to the composition and organization of elements that form a substance, meaning the disposition of electrons, atoms, layers and macroscopic appearance. Properties, in this case, are the set of responses to stimuli that matter with a determined structure display, such as emission and absorbance when excited with light and phase transitions after temperature changes. (1)

In this reasoning, natural materials and biomaterials are two of the classes of materials of interest in materials science due to their nature and applications. Some naturally formed materials are composites, formed by a combination of two types of materials. Examples of natural composites are wood and bone, that are a combination of an organic polymeric matrix that overlie a second material. Biomaterials are compatible with the human body and are fabricated for medical procedures, used in prosthetics and implants. (1)

Coral skeletons are a natural material and biological composite of interest, as they are formed both by organic tissue and a mineral, frequently calcium carbonate (also called limestone). Corals that form limestone skeletons are commonly reef builders, and provide scaffold for other marine organisms by modifying the ocean floor. (2)

Coral skeleton pieces can also be used as grafts in bone reconstruction due to suitable characteristics, such as porosity, composition and biocompatibility, leading also to biomimicry initiatives. (3) Moreover, coral skeletons have been proposed as a concrete enhancer, both in durability and resistance, hence modern composites for engineering applications have been modeled after biominerals. (4)

Reef formations and coral skeletons are known for outstanding mechanical performance, withstanding waves, tides, coastal storms at shallow waters (5) and high pressure at deep waters. This property is attributed to microscopic mineral building blocks organized in a three dimensional organic matrix that has naturally occurring twin boundaries, impurities and other architectural intricacies. (2)

On a macroscopic aspect, calcareous deposits left by ancient shallow water reefs are also useful for climatic mapping and reconstruction of past sea-level, as organisms that inhabit close to sea surface are normally adapted to the presence of light, warm temperatures and minimal suspended sediments, leading to a very narrow zone of optimal habitat. (6) Whenever this zone is no longer suitable for reef life, fixed organisms, such as corals, die and

leave a valuable record of traces and fossils behind. (7) This process, which has been natural and synchronous to Earth climatic cycles before the Industrial Revolution, has been severely affected by human activities and sea-level oscillations have been increasing in frequency due to Global Warming. Moreover, the absolute sea-level has been rapidly rising since the last Little Ice Age around 1850. Climate mapping, modeling and comprehension of past climatic conditions have become tools to predict and mitigate the effects of Earth's surface temperature rising. (8)

It is also notable that biological formations of limestone present differences from geological formation of limestone, both in the structure and properties in materials science context. Exemplified by slightly different crystalline lattice parameters (9,10) and very distinctive phase transition temperatures (10), to be further explored in following chapters.

Corals that form hard skeletons are a very diverse Subclass: Scleractinia (Bourne, 1900), with 1400 recognised species divided in 27 families, according to Kitahara *et al*. (11) Some species have had their skeletons studied individually and compared to geological calcium carbonate. But the present study will compare the structure and properties of two different coral species present in the brazilian fauna, *Mussismilia hispida* and *Lophelia pertusa*. Through a materials science perspective, these corals will be investigated for age, chemical composition, crystal structure and thermal behavior, and discussions will account for biological factors tied to specimens, such as morphology, clade, growth rate.

Finally this dissertation comprises the following chapters: literature review, samples and methodology, results and discussion. In literature review we will see basic coral biology, structure and properties of geological calcium carbonate and what is known about structure and properties of biological calcium carbonate. In samples and methodology, samples used will be presented, together with collection sites, and experiments chosen to investigate materials available. Results and discussion contain all results of experiments alongside some relevant results from the literature for comparison. Conclusions, project limitations and further steps close this dissertation.

2 LITERATURE REVIEW

2. 1 Overview on corals

Corals are part of the phylum Cnidaria, a very diverse taxonomic group of marine invertebrates with several representatives beyond corals, such as jellyfish and Portuguese man o'war. (12) The evolutionary history of Cnidarians start 740 million years ago during the neoproterozoic period, with soft bodied individuals. Hard tissue formation in cnidarians was not seen until 480 million years ago with skeletons made of calcite or chitin. The ancestors of modern corals were seen in fossil records from 445 million years ago, identified by the septa organization pattern. Corals proliferated and diversified significantly 250 million years ago together with the shift from calcite deposition to aragonite deposition, and the establishment of Scleractinians as the main reef-builders as seen today. These changes are highly correlated with dramatic climatic changes that Earth went through, namely formation of glaciers, CO_2 highs and perturbations of carbon cycles, among other phenomena. (13)

Organisms recognised as corals belong to the Subphylum Anthozoa which they share with sea anemones. Corals, specifically, are separated into two Subclasses Hexacorallia and Octocorallia (also comprising sea pens and). Differentiated by the subdivisions of their coelenteron, their mesenteries, multiples of six and incomplete septa for hexacorallians and eight complete septa that fully separate mesenteries in octocorallians. (12)

The corals used in this work belong to the order Scleractinia (Bourne, 1900) commonly referred to as stony corals, (14) called reef-building corals as they provide scaffold for other substrate-attached organisms and are capable of modifying ocean floor. (15) (15–17) Taxonomy explicit in Table 1.

Table 1 - Taxonomic classification of stony corals.

Kingdom	Phylum	Class	Subclass	Order
Animalia	Cnidaria	Anthozoa	Hexacorallia	Scleractinia

Source: Adapted from: HOEKSEMA; CAIRNS. (16-17)

The basic unit of mature hexacorallia (non larval state) is the polyp, which encloses all histological structures; a polyp can be defined as a stationary cylindrical body, covered with two layers of soft tissue, the epidermis and the gastrodermis, external and

internal tissues respectively. The space in between these tissues is the mesoglea, a gelatinous matrix composed mostly of non-living cells that may present sparse amebocytes with functions varying among digestion, antibacterial protection, wound repair and nutrient storage, alongside with some embryonary epidermis cells. (12)

The polyp has only one opening to the digestive system, which is a tentacle encircled mouth with food capturing function. This set of structures makes the oral disc. There are multiple tentacles, a number multiple of six. (12) The oral disc opens to the first element of the digestive system, the actinopharynx; leading to a second structure: an internal cavity called coenosarc, which is cut into mesenteries. The cylinder of the body is closed by an specialized epithelium layer called calicoblastic epithelium which is responsible for anchoring the soft tissues to the calcareous skeleton beneath it. (18-19)

A polyp basic elements are illustrated in Figure 1, each structural element labeled according to the description in the previous paragraph.

The defining trait of corals as belonging to the Phylum Cnidaria, is the presence of cnidae, or nematocysts, very complex organelles secreted in specialized cells called cnidoblasts that line the tentacles and gastrodermis of cnidarians. (12) Nematocysts, word of Greek origin, refers to a “bag of threads" which is quite descriptive of the nematocyst construction. The organelle is composed of a protein capsule closed by an operculum and filled with a coiled tubule that shoots out of the enclosure after being triggered by external stimuli. Nematocysts present varying functions, as they can deliver toxins, grab prey, adhere to surfaces for locomotion purposes. (20) Cnidarians are heterotrophs, as they acquire nutrients from the environment by capturing particles, plankton, or even phytoplankton through tentacles and speering types of nematocysts. (12,18)

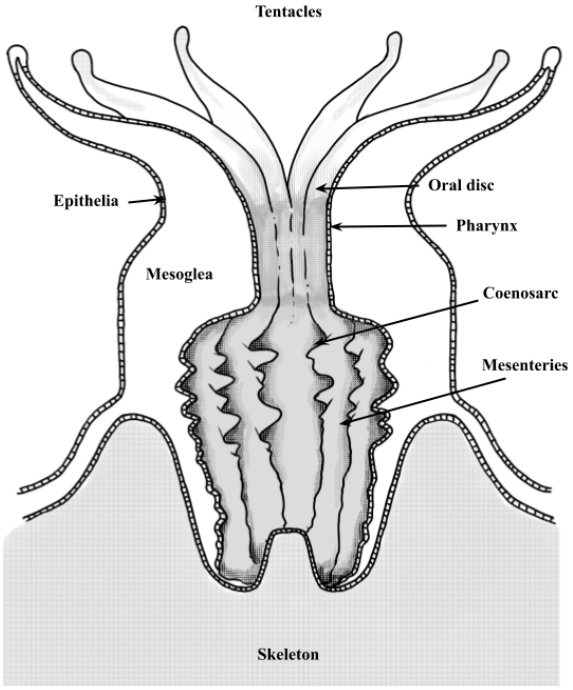

Figure 1 - Schematic view of polyp with labeled structures.
Source: Adapted from PECHENICK (12); Illustration by the author.

Moreover, symbiotic corals get a great fraction of their nutrition from its microbiome, as microorganisms provide alternative carbon sources through metabolites. Microorganisms, however, contribute far more to the metaorganism than feeding. (21) The symbiont organisms are specially relevant for reef-building corals called hermatypic or constructional, because the association with the dinoflagellate algae (zooxanthellae, genus *Symbiodinium*) favors the calcification through photosynthesis. (12,21-22) The main proposed mechanism for this phenomenon states that the energy barrier for $CaCO_3$ precipitation is lowered as CO_2 is captured, leading to a increase in pH. (23)

Corals can be either solitary or colonial, as being formed by one single polyp or multiple interconnected polyps. (12) Colonial corals can present various morphologies: glombose, ramose, branching, digitate plate, compound plate, fragile branching, encrusting, plate, foliate, microatoll. (24) A quantitative evolutionary analysis shows that corals present three clades, Basalia, Robusta and Complexa, that have diverged between 425 to 415 million years ago. (11,13)

Brazilian coral reefs differ from other reefs found in North Atlantic waters. Although these reefs present a smaller biodiversity when compared to the northern counterparts, having 23 species of stony corals, almost all species found in brazilian waters are endemic and predominantly of massive form. The “chapeirões” formations, columns in

mushroom form of aggregated coral that might reach 50 m wide and 20 m deep below surface water, found exclusively in southern Bahia. (25)

Coral habitats can vary substantially according to species adaptations. Reefs' presence extends from up at sea surface level, even being exposed to air during low tides, down to hundreds of meters deep where light no longer reaches. More precisely, corals can thrive between 0 m and more than 1500 m deep (7,26) The presence of corals in several different habitats is important for the ocean carbon cycle for the deposition of calcium carbonate. (27)

2.2 Structure and material properties of geological calcium carbonate

The collective term for lithified calcium carbonate polymorphs is limestone. (28) It is divided between calcite, aragonite and vaterite. Both aragonite and vaterite are metastable but the latter is hardly found at ambient conditions as calcite and aragonite. (29)

Geological aragonite, in particular, is the high-pressure polymorph of calcium carbonate (29), according to Figure 2, is formed ~ 3 bars, or ~300 kPa, at low temperatures. It is frequently found as the constituent of speleothems which are formed in caves and grottos from dripping water. Aragonite formation is favored by the molar ratio of Mg/Ca between 1.0 and 1.5 while calcite nucleation is inhibited. (30)

The natural formation of aragonite stalactites and stalagmites have shown that aragonite can be formed at relatively warm temperatures (>12 ºC) and atmospheric pressure. At 15 ºC, needle-like aragonite is formed by slow and constant water evaporation and degassing of cave environment. The evaporation effectively increases the concentration of Mg in the water, favoring aragonite nucleation. (31) The seasonal weather variations have shown to affect the deposition of aragonite in caves in China, forming laminae of aragonite. During winter a denser layer is deposited by moderate drip-water rate and constant slow degassing, and is then extended in spring, forming a porous layer related to lower drip-water rate and higher Mg/Ca ratios. (32)

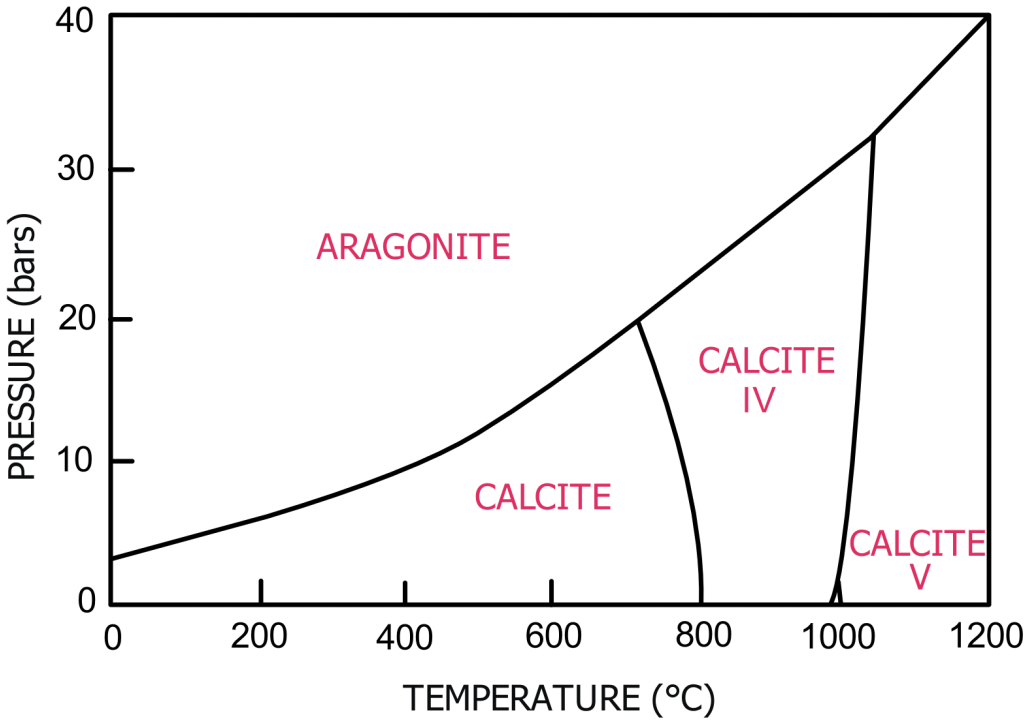

Figure 2 - Phase diagram of calcium carbonate polymorphs formation.
Source: Encyclopedia of Soil Science. (28)

Aragonite single layer was synthesized in laboratory at 30 ºC and 7.4 pH on surfaces submerged in both natural and artificial seawater for biomimetic purposes. (33) Another example of synthetic aragonite fabricated at ambient conditions shows that aragonite growth was favored by confined small spaces. A porous membrane was employed as scaffold for calcium carbonate synthesis, this setting showed that increasingly small pores increased the quantity of aragonite that grew. (34)

In respect to crystallographic data, aragonite was characterized with high precision by Caspi *et al.* (35) and Pokroy *et al.* (36) Both researchers used Synchrotron Radiation to conduct their experiments and defined aragonite is an anhydrous $CaCO_3$ polymorph, belonging to the Pnma (equivalent to Pncm) space group, which consists of an orthorhombic crystal system number 62 on Hermann-Mauguin. (33,35-36) The obtained dimensions for both geological and biological unit cells of aragonite, as well as geological calcite are displayed on Table 2, below.

Table 2 - Lattice parameters for aragonite and calcite of variable origins.

Phase	a (Å)	b (Å)	c (Å)	α, β, γ (°)	System
Biological aragonite	4.96524	7.96358	5.74842	90, 90, 90	Primitive orthorhombic
Geological aragonite	4.96183	7.96914	5.74285	90, 90, 90	Primitive orthorhombic
Geological calcite	4.9869	-	17.0496	90, 90, 120	Trigonal

Source: CASPI *et al.* (35); POKROY *et al.* (36)

2.3 Biogenic materials analysis

Coral skeleton structure is not a recent scientific interest and works dating from the late 19th century cover the basis of skeletal characteristics, differentiating coral species by porosity of the material. (37) Scleractinias were still called Madreporarians.

2.3.1 Structure and properties

Since the late 1950s scientists already knew coral skeletons were mostly aragonite and crystals could present micro, meso and macrostructure in regards to scale, from nm to μm. These discoveries were largely supported by the advancing of scanning electron microscopy. (38-39) By the beginning of the 1960s, some insights on deposition were obtained, as researchers started inferring if calcification happens equally in light and dark. (40) Coral skeletons were identified for having bands of different density as a function of water temperature and other environmental factors in the next decade. (39,41)

Some works pioneered the study of coral skeletons. The research by Gaffey *et al.* (42) investigates material behavior when facing annealing, drying and roasting, all common methods of sample preparation for other investigative techniques. They conclude that the coral skeletons, amongst other biogenic materials, present great behavior variation even in the same sample by measuring weight changes and NMR spectra for H_2O bands as OH^-. (42)

The crystallographic characterization of coral skeletons have been able to reveal the presence of an organic phase blended with the inorganic hard tissue since the end of 1990s and beginning of 2000s (43-44) A more refined study on the hard tissue benefited a lot

from modern techniques. For example, the presence of hierarchically organized crystals could be identified by a set of experiments comprising synchrotron radiation, laser assisted confocal microscopy and field emission scanning electron microscopy. The results indicated that skeletons are formed by nanoscaled grains, of 30-100 nm size, and connected by mineral bridges. (45) Besides, authors identified anisotropic properties on coral aragonite crystals, in agreement with works on molluscan aragonite (9,45)

Omer *et al.* (46) explores coral *Acropora cervicornis* mechanical properties, starting by differentiating samples by bleaching methods: one chemical and one biological. The chemical method consisted on the digestion of proteins and organic matter by 0.2M NaOH treatment, while the biological method involved samples being buried in sand so organic parts could be removed by microorganisms. Samples had their Vickers hardness, Young's modulus and uniaxial compressive strength determined. Values for chemically and biologically bleached were similar in all experiments: 3.7 ± 0.3 and 3.7 ± 0.3 GPa for Vickers hardness; 0.2 ± 0.2 and 0.3 ± 0.1 GPa for Young's modulus; 10 ± 2 and 14 ± 7 MPa for uniaxial compressive strength.

Studies on biogenic aragonite physical behavior and physical properties have been providing insights on what it differs from its geogenic counterpart. For instance, a research group from Hiroshima University have extensively examined thermal stability and nature of thermally induced transition aragonite-calcite, from synthetic to mineral and biological. The researchers were able to identify some key differences between abiogenic and biogenic aragonite thermal behavior. (47–50)

It was identified through thermogravimetric (TG) analysis coupled with mass chromatography that biogenic aragonites dehydrate in three separate steps in opposition to synthetic aragonite that presents only two dehydration steps. In particular, scientists evaluated that coral aragonite suffered phase transition between 250 and 300 ^{o}C, during the second dehydration step. The process is attributed to the expulsion of intercrystalline water, not found on aragonite from non-biological sources. (50) Both the TG and the mass chromatography shown in the paper are referenced below in Figure 3.

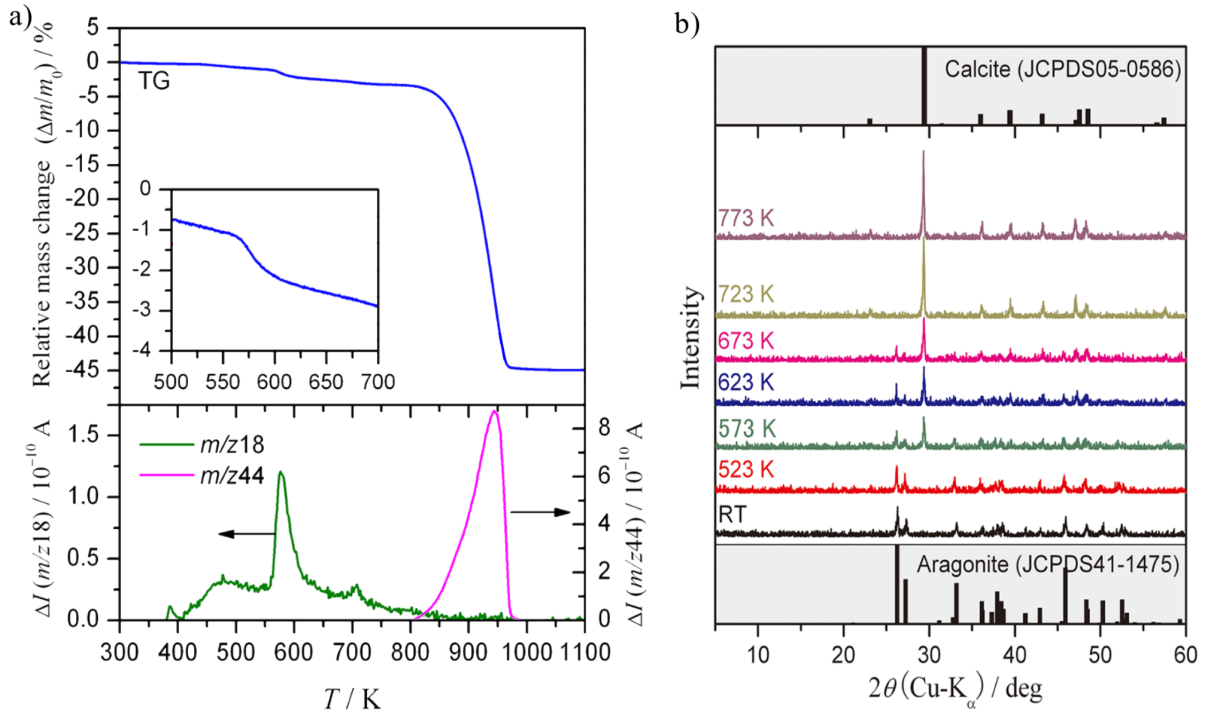

Figure 3 - a) In blue, thermogravimetric (TG) measurement in which mass is continuously measured in increasing temperature, assessing for disintegration of coral aragonite sample from *Pavona sp*. Thermal decomposition of CaCO3 is expected to begin at 650 ºC (823 K). TG is coupled with mass chromatography that separates released compounds by atomic mass, shown in green and pink curves. Green curve indicates release of water vapor, pink curve indicates release of CO_2; b) powder X-ray diffractometry for increasing temperatures, between 300 and 700 ºC. Diffractograms show the progression of phase transition from aragonite to calcite. Phase transition is completed at 450 ºC (723 K).

Source: Adapted from: KOGA; NISHIKAWA. (50)

Okumura *et al.* (10) has also shown that aragonites from distinctive origins present disparate temperatures for phase transition to calcite. The coral sample, especially, presented a much lower starting temperature for phase transition, around 290 ºC, than other aragonites studied, both biogenic and not. A very contrasting result to the phase transition starting temperature of geological and synthetic aragonites, between 400 and 450 ºC. (10) Figure 4 below summarize the analysis.

The same work (10) also evaluated lattice distortions by axial ratios (a/b and c/b) both prior and after treatments. It was found that, prior to treatments, aragonite deposited by marine animals were larger in a and c directions and smaller in b direction then a geological standard. After treatment, heated samples presented the same dimensions for a, b and c. The proposed mechanism for this phenomenon was that the incorporation of sodium ions (Na^+) as substitutions, along with the presence of OH^- or O^{2-}, and its consequential diffusion through lattice during heating caused the distortion and later the straightening. (10)

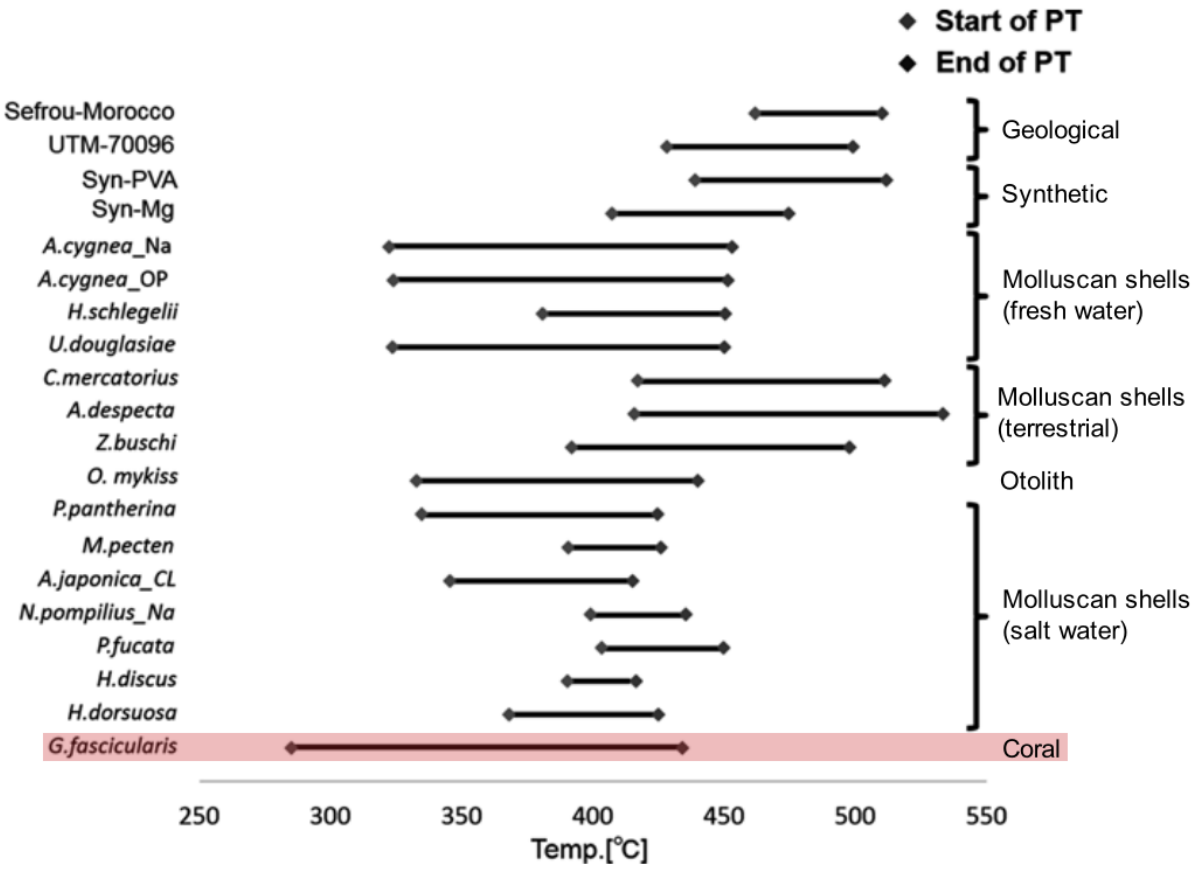

Figure 4 - Starting and ending temperatures of phase transition for aragonite to calcite for materials of different origins. Coral, *Galaxea fascicularis* highlighted in red.
Source: Adapted from: OKUMURA. (10)

Regarding chemical composition, aragonite can be either detailed for substitutions and impurities in the crystal lattice or presence of stable isotopes.

Neumann-Micheau and Tributsch (51) present an energy dispersive X-ray spectrometry (EDX or EDS) for clean coral skeleton and skeleton covered with organic matter, in both cases the main elements that constituted the sample were Calcium, Carbon and Oxygen. For the clean skeleton trace elements found were Sodium, Silicon and Chloride. When also considering the organic matter, trace elements found were Nitrogen, Sodium, Magnesium, Phosphorus, Sulfur, Chloride, Potassium and Barium. A table with element quantities was not shown.

Swart (52) analyzed the distribution of the most common trace-elements ingrained in coral skeletons: strontium, magnesium and sodium. Strontium is the most common contaminant in coral skeletons due to its proximity in radius to calcium and is the most relevant for this present research. Swart concluded that the deposited Sr^{2+} in the skeleton is directly, but somewhat weakly, related to the is Sr^{2+}/Ca^{2+} content in seawater and corals

present an increased growth rate. (52) This conclusion, however, appears as diametrically opposed to the chapter 4 on the Handbook of Stable Strontium, also from 1981, which covers strontium as an inhibitory competitor to calcium deposition. (53-54)

The presence of strontium and its distribution throughout the sample can be very informative as strontium partitioning in water is temperature dependent. BECK *et al.* (55) uses strontium to assess sea-surface temperature (SST) from the last 100 thousand years, identifying it to be 5 ºC lower than today's SST. Similarly, a 1997 study says that strontium might be incorporated into calcium carbonate polymorphs not only as substitutions but also as an alternative phase, as they would cluster and form $SrCO_3$, strontianite, ingrained in $CaCO_3$. (56)

In 2012, benefiting from technological improvements, researchers addressed the presence of contaminant cations by nanoscale secondary ion mass spectrometry (nanoSIMS). Brahmi *et al.* (57) also propose that the dynamics of biomineralization is oftentimes responsible for non-uniform deposition of impurities. They identify regions of rapid accretion and slow accretion, which differ in composition primarily in magnesium content (Mg/Ca), 13 mmol/mol and 2.2 mmol/mol respectively. Although strontium content was also assessed, the authors did not conclude that its content is so directly related to skeletal deposition. However, the main conclusion is that corals have great capacity for controlling skeleton accretion in time and space. (57)

Being known that corals are great environmental recorders, and for quite some time now, scientists have been able to connect oxygen stable isotope ratio $^{18}O/^{16}O$ to temperature. (55-56) A brazilian research group studies the growth rate of *Mussismilia hispida* as means to establish if the species is suitable for environmental recording. Authors conducted experiments of uranium-thorium series for aging assessments and compared these results to $\delta^{18}O$ ($^{18}O/^{16}O$) and $\delta^{13}C$ ($^{13}C/^{12}C$) obtained with mass spectrometry. They were able to measure not only growth rates of three different colonies (all ~3±1 mm/year) of coral but also tie these results to short-term and medium-term variations of skeleton deposition, translated respectively to a yearly cycle and a decadal cycle, concluding that *M. hispida* is a precise token for climatic analysis and reconstruction. (58)

One of the major problems of using corals and metastable minerals for climatic reconstruction are the effects of time and the prevalent changes it causes. Then, diagenetic effects must be taken into consideration (59-60) Especially on the tangent of paleoclimatic reconstruction, as substitution of primary aragonite by 1% of calcite or by ~2% mineral aragonite is capable of distorting temperature assessments up to +1 ºC or down to -0.9 ºC,

respectively for calcite and aragonite contaminants. This distortion is mainly caused by disruption of Sr/Ca ratios on fossilized materials. (61)

Diagenetics effects over aragonite are its dissolution and substitution for a modified cement, such as low or high-magnesium calcite or secondary aragonite with microstructure differentiation. Type of cement mostly influenced by the surrounding medium and primary phase. These diagenetic processes are recognized both for biological and geological aragonite. (62-63) Microstructural changes were mostly pointed out by studies on biological aragonites in which the crystallite surface, once smooth, starts to present spicules. (64)

Sayani *et al.* (62) and Hendy *et al.* (64) show important microstructural changes and surface-level identifiers of diagenesis on *Porites* coral skeletons by SEM images and dating methods, such as Sr/Ca and U/Th. Sayani *et al.* (62) approaches diagenesis and dissolution by identifying regions of aragonite dissolution and concomitant recrystallization of the immediate surface, generating a coating of distinct morphology. Hendy *et al.* (64) reports surface etching by weak acids, such as HNO_3, and consequent exposure of structures underneath the first layer or, maybe, the sealing layer of aragonite. (64) Both can be seen on Figure 5.

Diagentics has been reported to affect corals as young as 30 years old. Is discussed that the typical alterations on structure, for any mineral exposed to weather, are dissolution of the primary phase, infiltration of a secondary cement and recrystallization of the primary phase. (62)

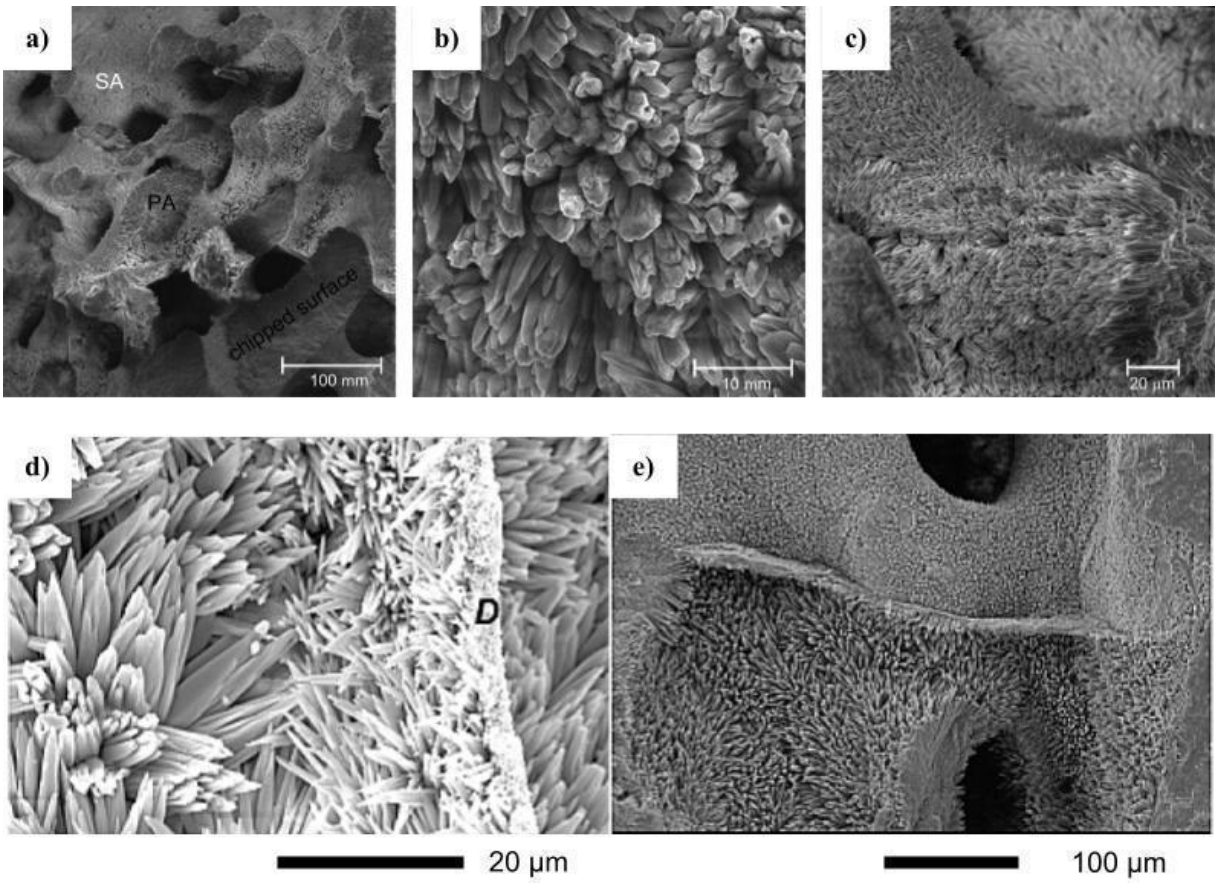

Figure 5 - SEM images of *Porites* coral skeleton surface, a) rod-like and acicular cements divided in primary aragonite (PA), secondary aragonite (SA) and chipped surface from the cutting process for a 400 year-old coral sample, SA surface is marked by a spiculed surface made of aragonite needles; b) magnified region of SA in a), evidence of acicular aragonite formation; c) acicular SA found in surface of 350 year-old coral sample with more densely packed needles; d) SA needles on a skeletal dissepiment (D) which separates layers of growth; e) frontier between PA and SA divided by dissepiment, SA is present below dissepiment while PA is above.
Source: Adapted from SAYANI *et al.* (62), Figure 6 and HENDY *et al.* (64) Figure 3.

Nguyen *et al.* (65) studied more profoundly the transformation implications of aragonite to calcite for climatic reconstruction, and although their work focused on mineral aragonite, it is suitable to be presented. The first proposition of the article is to quantify the retention of Mg/Ca, Sr/Ca and $\delta^{18}O$ during phase transformation. Aragonite samples were heated in the presence of NaCl solutions between 120 ºC and 184 ºC. The process revealed that transition to calcite occurs progressively starting from rims and cracks while core might still retain aragonite phase, however, some samples were fully transformed within 30h. Finally, the isotopic analyses demonstrated that calcite retains the $\delta^{18}O$ from the water, but Mg/Ca and Sr/Ca were partially or completely maintained.

Jonas *et al.* (60) has explored and replicated hydrothermal habitats and its effects on aragonites of several origins: abiogenic natural, bivalve shell and coral. Scientists

focused on the thermally induced replacement of aragonite in the presence of a high-concentration saline solution, in particular its reaction with 0.9 $MgCl_2$ at 200 ºC. The experiment caused the replacement of aragonite with several polymorphs of $Ca_{(1-x)}Mg_xCO_3$, ranging from low-Mg calcite and high-Mg calcite to dolomite and transitional phases. This paper contributes to elucidating the diagenetic process of limestones and carbonates, transformation rates, and materials characteristics that influence weather action over its structure.

Then, the calcite contamination on coral skeletons reported by Allison *et al.* (61) was not found to be a substitution but a parallel growing structure that infiltrated the skeleton pore space and coated the available surface presenting microstructures such as micrite or rhomb, and neomorphism, i.e., direct transformation of aragonite to calcite was not observed. Even though calcite can in fact substitute aragonite, exemplified by the formation of neomorphic calcite after nacre on fossilized cephalopod moulds. (66)

It is important to note that fossilized materials can have their initial structure preserved, and some contain what could be interpreted as diagenesis. A fossil of *Coelosmilia* sp., a coral species dating back to the upper Cretacious, roughly 70 million years ago, revealed that the carbonate polymorph that composed the skeleton was in fact biogenic calcite. (67) Similarly, in 2021 was reported the existence of a modern coral belonging to the antarctic region and profound depths with a two component skeleton, a aragonite shell filled with calcite. (26) It is important to highlight that both of these corals were described as Scleractinian, which most commonly deposit aragonite, and neither belonged to the subclass Octocorallia that knowingly deposit calcitic skeleton. (68)

2.3.2 Coral growth mechanisms and adaptation

Przeniosło *et al*. (45) studies microstructure of coraline aragonite differentiating by accretion rates: rapid accretion deposit (RAD) and thickening deposit (TD). RADs are agglomerates of randomly oriented aragonite crystallites ingrained in organic matrix that initiate the growth of TDs in bundles of fibers or needles, that spread similarly to a fan, as can be seen in Figure 6. RADs are frequently found as synonyms for centers of calcification.

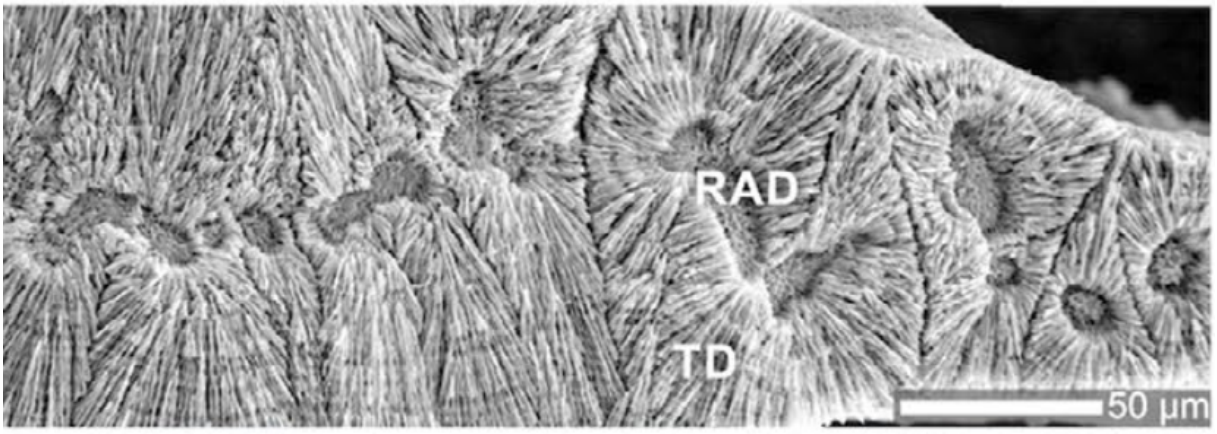

Figure 6 - Discrimination of growth regions between rapid accretion deposit and thickening deposit on coral skeleton.
Source: DRAKE *et al.* (13)

Mollica *et al.* (69) also proposes a two step model of growth, dividing it in extension and densification, meaning upward growth and lateral growth respectively. According to the work, when facing acidic environments, corals of genus *Porites* maintain their extension rates but not their densification rates.

Mouchi *et al.* (70) report the usage of electron backscatter diffraction as a method to study biominerals. Authors investigate the skeleton formation of *Lophelia pertusa*, also making the distinction between RAD and thickening deposit TD. Through the study, they revise the explanation for the origin of opaque and translucent bands by texture conceded by growth direction of fibers, commonly thought to be related to water temperature. The study's main focus relates to climate change and coral resilience, as authors try to understand the strength of coral skeletons when facing waves.

As seen in Figure 7, the banding presents distinctive preferential growth directions, and this tendency is likely tied to the development of sclerodermites, an ultrastructure composed of aragonite. Mouchi *et al.* (70) argue that RADs do align at the edges of translucent-opaque bands perpendicular to the coral wall and form the prime layer of growth, leading to aligned regions of more developed sclerodermites, which form a translucent band. Then the opaque bands are formed by less developed and scattered-grown crystals.

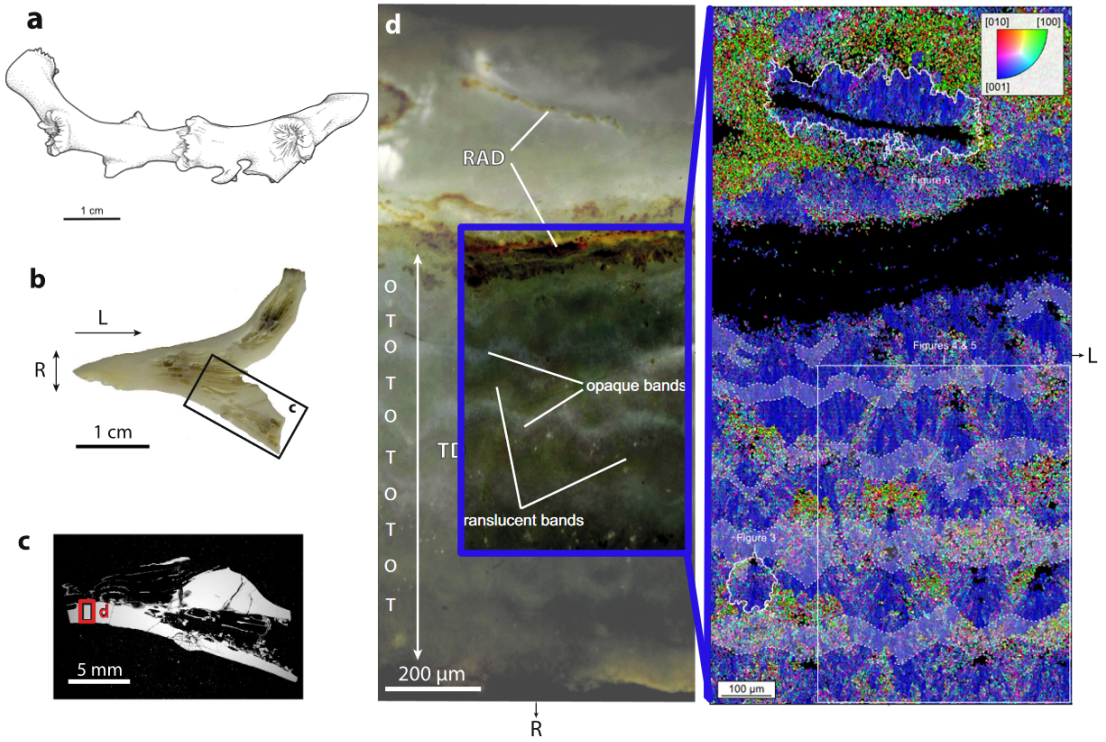

Figure 7 - a) Illustration of *L. pertusa* specimen. Starting in (b) all images are progressive enlargements of interesting sections; b) photograph of cut *L. pertusa* fragment; c) micrograph of interest area in *L.pertusa* branch; d) Reflected light image of RAD and TD. Opaque (O) and translucent (T) bands are indicated. To the right, an EBSD shows the crystal growth based on direction indicated by color: blue is [001], red is [010] and green is [100].
Source: MOUCHI *et al.* (70); compiled and edited by the author.

Sun *el al.*, (71) approaches coral growth from two perspectives: experimental and computational, to study skeleton formation across species, more specifically nucleation and formation of spherulites. For this, scientists identify crystal orientation of deposited materials through polarized-dependent image contrast, or PIC, aided by photoemission electron spectromicroscopy. They have proposed a mechanism for spherulite formation. Authors say that the ultrastructure starts with a bundle of randomly oriented equant (not-elongated) crystals and support their mechanism with thermodynamic simulations, as well as references that have seen similar phenomena for different materials, like cocoa butter, opals and graphite in cast iron.

On a more biological approach, skeletal synthesis is proposed to happen in a privileged space outside the cell filled with an extracellular calcifying fluid (ECF). This is an ion saturated fluid that is able to precipitate amorphous $CaCO_3$ that later crystallizes in aragonite or calcite. (72)

It has two more main proposed aggregation mechanisms for $CaCO_3$: particle attachment (PA) and ion attachment (IA). (73) The PA is a considerably faster growth

mechanism than IA. PA is limited by sphere packing problems as complete charge-neutral particles of $CaCO_3$ do not join and occupy 100% of a given space. Thus, the proposed mechanism says that cells of biomineralizing organisms produce ECF that starts the PA and the mineral grows further by IA that fills the remaining interstitial spaces, intermediated by proteins and other biomolecules as organisms might control the deposition of the skeleton. (72-73)

Malik *et al.* (74) explored coral adaptation to a changing environment mainly through *Stylophora pistillata* colony transplant from 5 m depth down to 60 m, i.e., euphotic zone to mesophotic zone. Adapted corals displayed changes in skeleton formation, disclosed in Figure 8. It was noted that corals originated from shallow water presented skeletal growth in a fan-like pattern, irregular but denser dissepiments, while corals from deep water presented a more uniform distribution of dissepiments and appeared less dense in skeletal central region.

Also adaptation can be exemplified by porosity. Corals from mesophotic zones were 17% more porous than euphotic corals. After transplantation, corals originally from deeper waters showed a porosity decrease of 8% in 15 months, while corals from shallow waters originally increased the inner-skeleton porosity by 3%. The standards for these values are non-transplanted control colonies. (74)

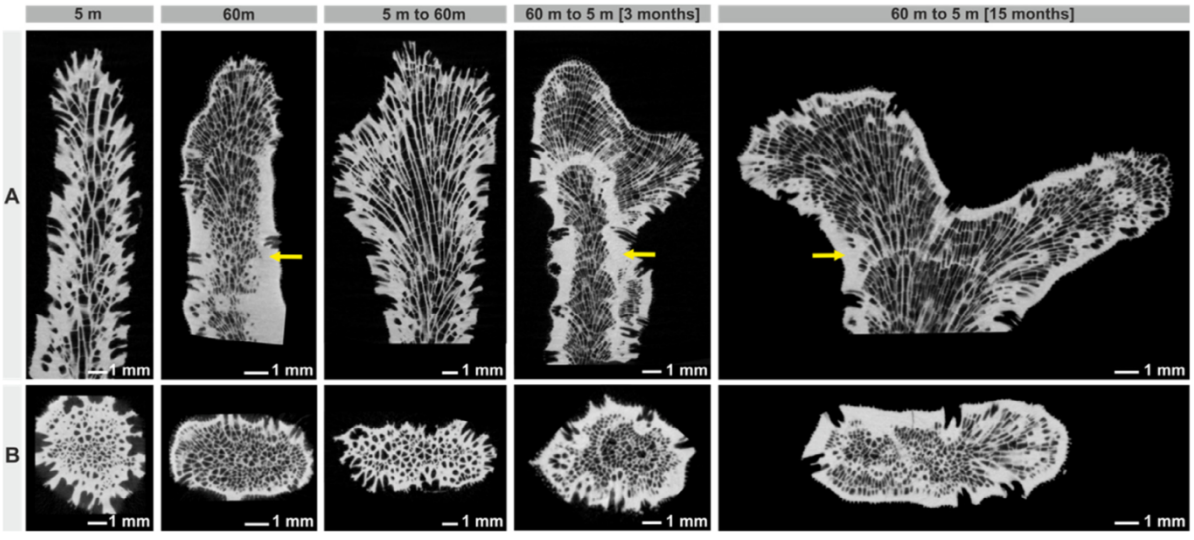

Figure 8 - Micro-computed tomography (μCT) scans of transplanted *S. pistillata* corals A) in a longitudinal cut and B) in transversal cut 0.5 mm from coral tip. Yellow arrows indicate thicker skeletal formations of corals from 60 m depth both originated and transplanted. Analysis shows that internal divisions of skeleton, septa, are more evenly formed in deeper waters along with thicker external walls in opposition to non-uniform septa and thinner walls in shallow water.
Source: MALIK *et al.* (74)

2.4 Summary

In summary, corals have evolved to deposit aragonite in the last 250 million years. It has been proven that biological aragonite has different physical properties than geological aragonite, such as: distinct phase transition temperatures and particular form of growth. The latter is especially interesting due to the useful bands of different densities that are seen, even more for the presence of isotopes and ions such as ^{18}O and Sr^{2+} that indicate sea surface temperatures for a given time. There are new insights for the existence of these growth bands, interspaced opaque and translucent form a crystallographic point of view, in which bands appear according to the main crystalline direction present at that section. The observed microstructure of a biological aragonite is relevant to assess age and adaptations to the environment. The full mechanism of how corals are able to synthesize aragonites that differ from its geological form is still not fully understood.

3 SAMPLES AND METHODOLOGY

This work conducts a comparative analysis of their physic-chemical properties, evaluating how aragonites from distinctive origins behave under a material science light and how environmental factors can impact the material. We are aiming to investigate chemical composition, thermal stability, crystal structure while maintaining in sight the different backgrounds that samples provide. For this purpose, physical techniques were employed as the primary assessment while comparison with literature and deposition mechanisms inferred by the latter are a secondary assessment of samples available.

3.1 Sample collection and description

Sample collection location is summarized in Table 3. *Mussismilia hispida*, was collected in 2013 from a near-shore reef at Praia do Príncipe, Ilha Trindade and placed directly in alcohol after being removed from water. This coral is also complete and presents some substrate still adhering to its sides and soft tissue still covering its calices. *Lophelia pertusa*'s fragments were retrieved by a core, which consists of a hollow drill that penetrates the ocean floor and is progressively filled with material as it deepens in the soil. Locations are shown in Figure 9.

Table 3 - Site collection, condition of samples and preservation method.

Species	Latitude	Longitude	Depth (m)	Status	Preservation method
Mussismilia hispida	-20° 31' 48"	-29° 18' 54"	10	live	70% isopropyl alcohol
Lophelia pertusa	-24° 37' 48"	-44° 0' 36"	852	fossilized	dry

Source: Information provided on sample collection labels; MZ-USP.

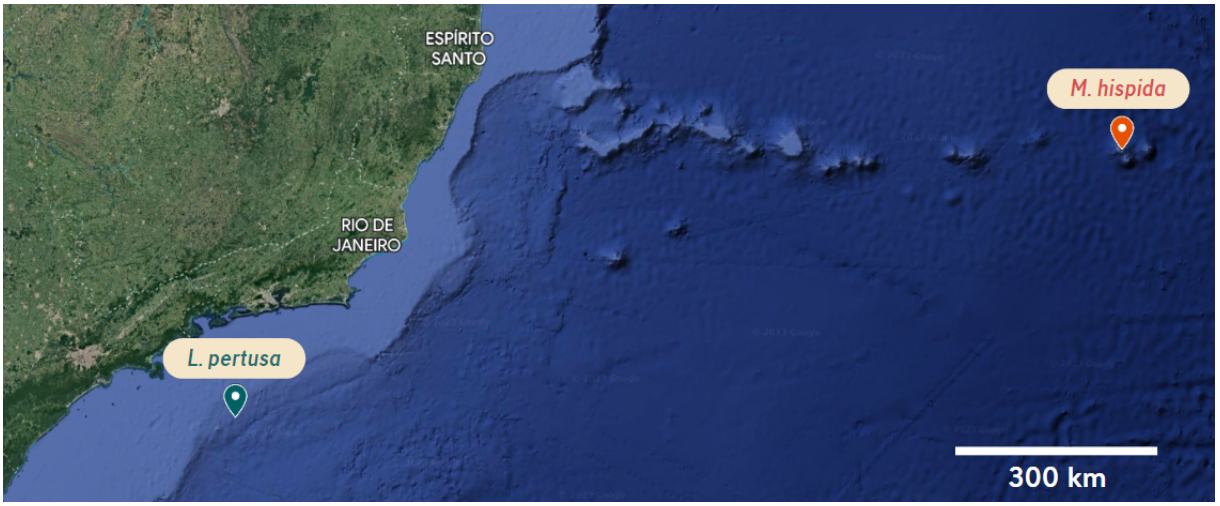

Figure 9 - Map of collection sites per sample according to coordinates.
Source: Satellite image from Google Maps.

3.1.1 *Mussismilia hispida* (Verrill, 1901)

Mussismilia hispida, Figure 10 - a, is a species of stony coral commonly found in the South Atlantic Ocean on seamounts and knolls. (16) It is present in a great portion of the Brazilian coast and particularly abundant in warmer regions, as it is found between 3° 51' 36" S (Fernando de Noronha) and 23° 7' 48" S (Rio de Janeiro). Also, the genus *Mussismilia* inhabits the shallow photic zone and has been reported to be found and collected from reefs between 1 to 30 meters deep. (16,75-76)

This species consists of a hermatypic, symbiotic, massive and colonial type of coral. Colonial corals are a contiguous mantle of polyps linked together by the coenosarc, a structure that connects one individual polyp's gastric cavity to the adjacent one, belongs to the clade Robusta. (11,77)

3.1.2 *Lophelia pertusa* (Linnaeus, 1758)

Lophelia pertusa, Figure 19 - b, has been reported to inhabit from 40 m to 2775 m of depth and is considered a cosmopolitan species due to its dispersion through the globe. (78) Although *L. pertusa*'s population is larger in the North Atlantic, it is found on South Atlantic coasts between 17º 25' S (southern Bahia coast) and 34º 30' S (northern Uruguay coast). (17,79)

L. pertusa is a branched colonial coral mainly found on cold and/or deep waters, and even though it is capable of sustaining other forms of life in bioherms by forming deep-sea carbonate mounds, it is considered constructional but ahermatypic because the species is not reef forming. (22,80) Even though *L. pertusa* is depleted of zooxanthellae and other photosynthesizing microorganisms, the species has symbiotic bacteria. (80)

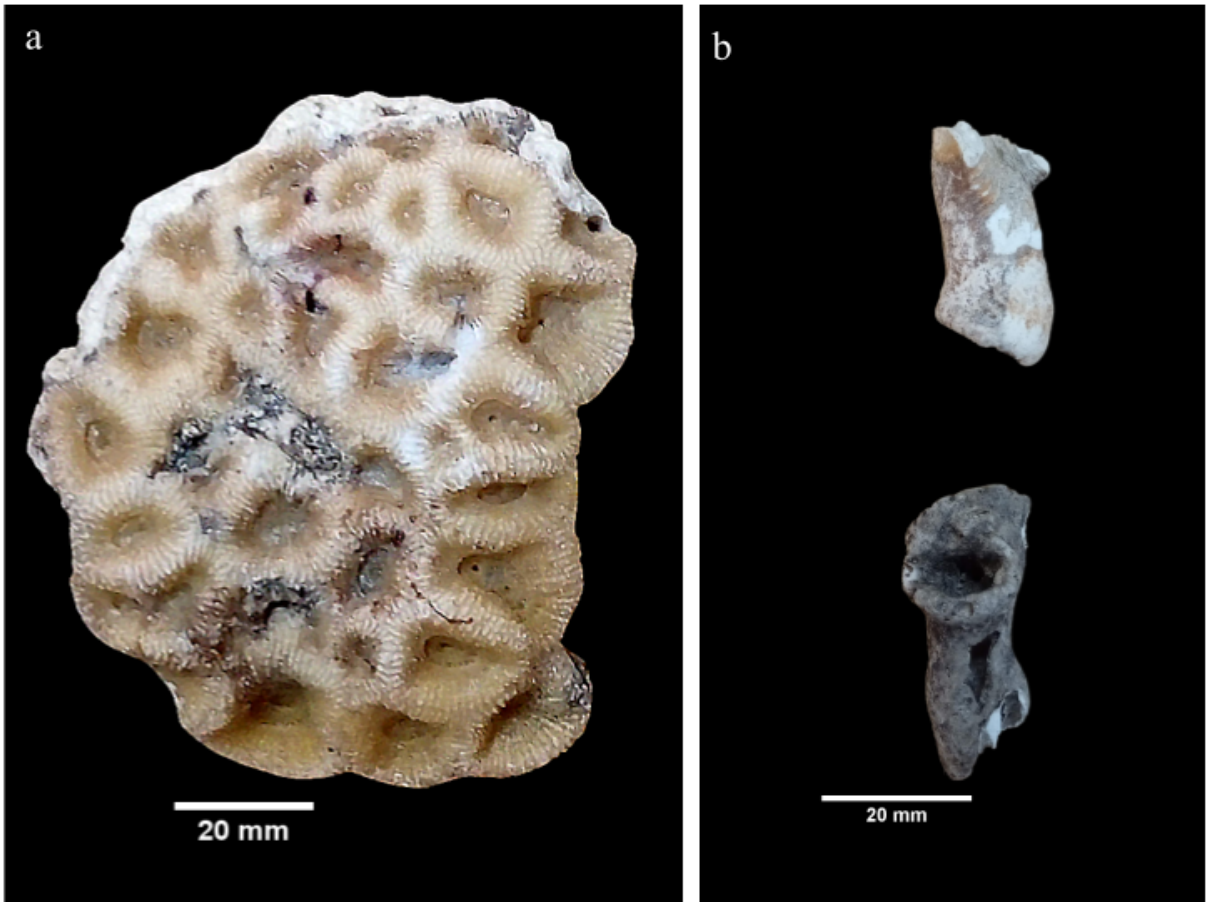

Figure 10 - Photograph of a) *Mussismilia hispida*, b) two fragments of *Lophelia pertusa*.
Source: By the author.

3.2 Sample preparation

Both species had to be prepared prior to experiments. Mostly, they had to be cut, grinded and separated for the following analysis. The cutting step was made with a circular diamond saw with a micrometer scale allowing cut thickness control. Cutting trials showed that the minimum thickness for samples is ~3 mm, as the porous regions crack when cut below this margin and compromise the sample's integrity. Slicing samples on the precision

saw required attaching to a glass plate often made with non-permanent epoxy glue or bee's wax.

The following cleaning and washing steps had to be performed with either ketone or isopropanol to remove the remainders of adhesive. Samples were then rinsed in tap water and finally washed with distilled water. Next, samples could be either air-dried at room temperature for ~24h or dried in the incubator at 100ºC for ~2h. The drying step also removes the excess solvent from adhesives.

Samples were assessed for densities by the Archimedes method using the scale accessory kit. Three subsamples of each coral were analyzed for their densities.

If grinding is necessary, samples would be powdered with an agate pestle and mortar, and then sieved to suitable grain size. Grain size was frequently selected between 75 and 90 μm, or 180 to 200 mesh. Finally, samples can be separated in 1 ml microtubes and directed to experiments.

Thermal treatments can be an additional preparation step for further analysis. They are a necessary process for dehydration and removal of organic matter and also can provide insights on material stability and behavior.

Treatments employed were carried on a digitally controlled furnace. The standard heating rate applied for all thermal treatments was 10 ºC/min. Samples went through the following treatments: 200 ºC/2 h, 260 ºC/1 h, 285 ºC/1 h and 400 ºC/2 h. These treatments were applied to a range of subsamples and are specified before each result is presented. The main purpose of thermal treatments is to investigate stability, phase transitions and clean samples of organic matter.

A chemical treatment was used to remove organic matter, consisting of a NaOH solution at 0.2 M. The solution was applied at a ratio of 1.5 mg of sample for each 1 ml of solution. The aqueous solution of NaOH (and other alkaline solutions) are suitable for removing organic matter as it precipitates by being neutralized and broken. Na^+ neutralizes negative charges of organic matter and OH^- breaks the hydrogen bonds. This protocol was adapted based on molecular biology protocols (81) and later confirmed by (46).

Chemical etching was used for improving visualization for supporting microscopy images by defining single crystals edges. Etching was performed with citric acid 0.3 mol/L for 1 min, 30 min and 60 min, following the protocol by XIE *et al.* (82)

3.3 Energy Dispersive Spectroscopy and Scanning Electron Microscopy

Energy dispersive spectroscopy (EDS), is a technique for elemental composition analysis, based on specific X-rays response from elements after excitation. This experiment was conducted on powdered samples with particles sieved to be between 75 and 90 μm arranged in a small tablet over carbon tape, later covered with a platinum layer. The results presented in this work were collected at LMEA, IFSC/USP, with a Zeiss Sigma scanning electron microscope coupled to an Oxford chemical analysis system capable of detecting elements between Borum and Uranium. EDS collected data that were equal or smaller than the associated detection limit and error were disregarded and will be presented exclusively in Annex A alongside resulting spectra.

The scanning electron microscopy was performed at a Hitachi TM3000 Tabletop Microscope at 5 kV with no need for metalization as the equipment performs measurements under vacuum. Samples were placed over a stub covered with conductive carbon tape. In this work, SEM images allowed for microstructure characterization.

3.4 Radiocarbon dating

Dating samples required only clean slabs of coral to be sent, as samples need to be graphitized and processed at the CENA/USP facilities prior to measurements. Radiocarbon measurements were conducted at the Center of Applied Isotope Studies, department of University of Georgia (USA). Total ^{14}C content was assessed with an NEC Acceleration Mass Spectrometry (AMS) and data returned were further calibrated to fit the atmospheric carbon content in function of time, as it has not been constant through eras. By this process ^{14}C dating will be given in terms of probabilities with trust intervals of 1σ (68%) and 2σ (95%). (83,84)

Carbon dating report returns the following data for each sample analyzed: percent of modern carbon (pMC), age, calibrated age and average probability.

pMC, refers to percent of modern carbon. This data is a comparison to the carbon year zero, 1950, by which all samples are calibrated in relation to. It is a sample of known age that represents the 100 on the pMC scale and all other examined samples are fractionated and placed on the scale regarding it. (83)

Age, presents an uncalibrated age of samples, which means the radiocarbon age in years before present, more commonly denoted BP. Carbon isotope content in the atmosphere is not constant through time, so what the second column expresses is the age in reference to radiocarbon years before present (RCYBP or simply BP), parallel to calendar

years, not opposed to. This age measurement is accompanied by a 1σ precision, which represents a 68% probability. Notice that the σ values are not tied to the experimental error in this case, and refer to the certainty interval of age, as RCYBP dating are denoted by a probability distribution around the measurement. (83)

The described calibration is illustrated in Figure 11.

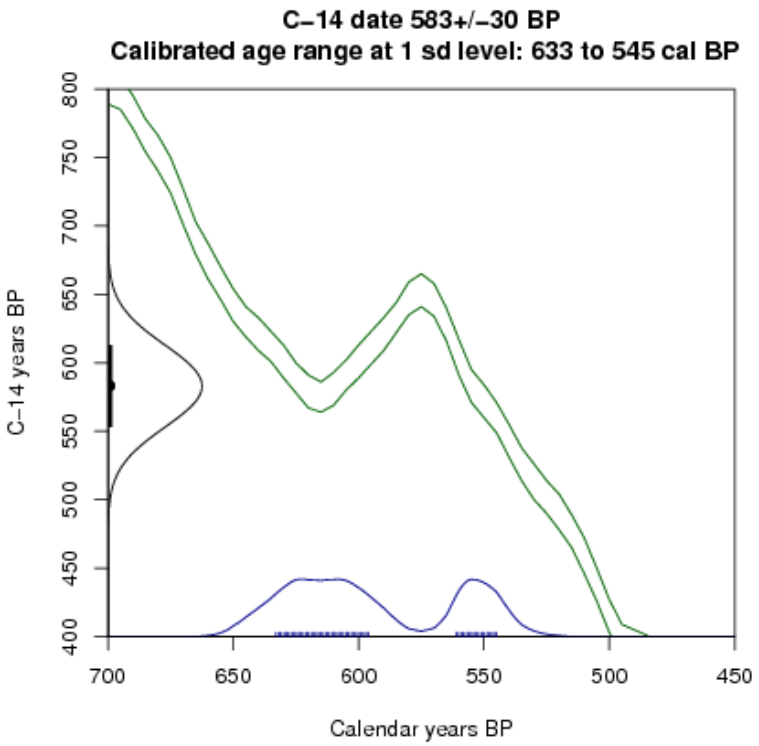

Figure 11 - Example of calibration curve graph for interpreting radiocarbon years in calendar years.

Source: Texas Beyond History website, Interpreting Dates. (83), edited by the author.

Calibrated age, refers to the post processed data of ^{14}C quantification, and is given in calendar years, converted to conventional time measurements. This data is reported with 2σ (95%) probability factor. Average probability simply refers to the mean value of the calibrated age. (83)

3.5 Thermogravimetric analysis

Thermogravimetric analysis (TG) investigates the thermal stability of samples by measuring mass changes throughout a temperature gradient. In this work, samples' behavior were collected by Netzsch TG 209 over a platinum crucible. Thermal reactions happened in an Argonium inert atmosphere with 1 ml/min flow rate and Nitrogen purge gas at

10 ml/min flow rate, while temperature was continuously increased at a 10ºC/min rate between ambient temperature up to 800ºC.

In order to investigate the nature of reactions, if reversible or irreversible, we employed a two step analysis. The first step samples were heated at conditions cited above, from ambient temperature up until 520ºC. Samples were allowed to cool down until ~100ºC, from where the second heating step took off and samples were heated until 900ºC.

To obtain mass variations in specific intervals, it was taken the derivative of curves and their integral after. This was made using Origin 2019 software and SciPy Python package Savitzky-Golay Filter function.

3.6 X-Ray powder diffraction

X-ray diffractometry is a powerful technique for assessing crystal structure, phase and phase fraction, especially when coupled with refinements, like the Rietveld methods for instance. Samples in this study were analyzed with a Rigaku Ultima IV X-ray diffractometer from 20º to 80º, in 0.02º increments, with 5 seconds of scan time per point. Further analysis was conducted on GSAS-II, a python based software that allows a comprehensive investigation of diffraction data, performs Rietveld refinement and simulations of crystal structures. (85) For data refinement, the parameters assessed were background, microstrain, atom position and unit cell dimensions.

4 RESULTS AND DISCUSSION

4.1 Carbon dating

^{14}C dating revealed that samples from deep water, fragments of *Lophelia pertusa* (*Lp*), are in fact remarkably old and present an average age probability of ~11950 years old while the shallow water sample, *Mussismilia hispida* (*Mh*), is only 22 years old, establishing in the year 2000 and being collected around 2014. Table 4 displayed dating per sample.

Table 4 - ^{14}C quantification and dating.

Sample	Laboratory Number	pMC	Age (BP)	Calibrated age (2σ; cal BP)	Average probability
Lp A	UGAMS#59324	26.952 ± 0.133	10532±39	11753 - 12166	~11933
Lp B	UGAMS#59325	26.876 ± 0.126	10554±37	11764 - 12184	~11972
Mh	UGAMS#59326	109.88 ± 0.341	-	23 - 21	22

Source: Compiled by the author. CENA/USP result reports.

The pMC content shows that *Lophelia pertusa* samples have gone through almost two cycles of ^{14}C half-life, 5700 ± 30 years. The implications of the time spent buried on soil are, as reported, the dissolution of primary aragonite and partial or complete transformation to calcite, (60,61) the degradation of organic matter and digestion of protein content. (46) It is also notable that sample *Lp* B presents a burned-like surface, plausibly tied to the colonization of soil by sulfur-oxidizing chemolithotrophic bacteria that produce sulfuric acid. (86,87) Samples indeed did not present any organic matter or soft tissue cover.

The resulting ages for *Lp* fragments set them in two possible time epochs: Holocene or Pleistocene. While Holocene comprises the last 11700 ± 99 years, Pleistocene started 2.6 million years ago, which lead it to be divided into subseries, Early, Middle, Upper Pleistocene. The Upper-Pleistocene being the shortest of the subseries and spanning from 126000 years ago to the beginning of the Holocene. (88) Accounting for this boundary, *L. pertusa* samples can belong to either epochs, but the average age probability being more than

11900 years, it is already past the trust margin of the Holocene dating. *Lp* samples will be considered as belonging to the Upper Pleistocene epoch.

4.2 Samples at eye level

Both samples were initially assessed for their dimensions and mass, which can be seen in Table 5. Apparent volume of samples was measured using images aided by ImageJ and Archimedes method. *Lp* apparent volume was preferentially measured by software to avoid sample manipulation, as the fossil is very fragile. *Mh* apparent volume was measured by Archimedes methods and later confirmed by imaging analysis. *Lp* is significantly less abundant for experiments than *Mh*. The dimensions of length and calyx diameter are not applicable for *Mh* geometry.

Table 5 - Samples macroscopic characteristics.

Sample	Mass ± 0.001 (g)	Length (mm)	Calyx diameter (mm)	Apparent volume (cm^3)	Skeletal density (g/cm^3)
Mh	171.2140	-	-	351 ± 1	2.03 ± 0.02
Lp A	5.0661	33 ± 1	15 ± 1	7.8 ± 0.5	-
Lp B	4.5904	40 ± 1	16 ± 1	8.8 ± 0.5	2.22 ± 0.02

Source: By the author.

For comparison, the work of Walsh *et al*. (89) compares the skeletal density of branched and massive corals and shows variability, branched species studied have densities between 2.232 to 2.835 g/cm^3 and massive between 1.787 to 2.815 g/cm^3. Also, their work discusses

Now that samples' age is known, it is possible to estimate coral growth rates based on dimensions. While *Lp* is only fragments of a larger specimen it is not possible to tell overall colony growth, but based on literature analysis, it is possible to infer time required for these particular fragments to grow to the seen size. Breeze *et al.* (90) reported that a 1.5 m tall *L.pertusa* colony can be ~360 years old. Some reported growth rates for *L. pertusa* average linear growth rate lies most frequently between 10 and 14 mm/yr, but can reach 26 mm/yr, in which case the polyp budding is an yearly process, and each polyp represents a full year of

colony's growth. (91–93) In these cases, each fragment took ~3 years to grow to their actual size.

The calyx diameter of both fragments lie between values already reported in the literature: 10 ± 2 mm for colonies in the North Sea (93), and 5 to 20 mm for *L. pertusa* colonies from reefs in southern Bahia, brazilian coast. (94)

Mussismilia hispida sample can have its growth rate directly calculated regarding that it has been collected after 13 years after settlement. The coral presents 42 ± 1 mm in height, growth axis measured according to SILVA *et al.* (2019) (58), leading to a 3.23 mm/year of growth rate, consistent with other studies on *M. hispida* growth rates on the South Atlantic Ocean (3.2 ± 0.7 mm). (58)

The skeletal densities measured for *Mh* and *Lp*B revealed 2.03 ± 0.02 and 2.22 ± 0.02 g/cm^3 respectively. If compared, densities measured and calculated with mass and apparent volume differ significantly due to pores and other cavities counted in apparent volume. *Lp* samples have a deep cavity where the polyp soft tissue used to be allocated.

Also, by investigating samples at eye level, it is also possible to infer the positions of each fragment, here as in the middle of the branch or the tip of the branch. *Lp* fragment B presents a bifurcation signifying that it was budding a new polyp indicating it to be a not so young or new; while *Lp* fragment A is the tip of a branch and has no bifurcation, and resembles a younger polyp, taking Maier *et al.* (92) as reference as it can be seen in Figure 12.

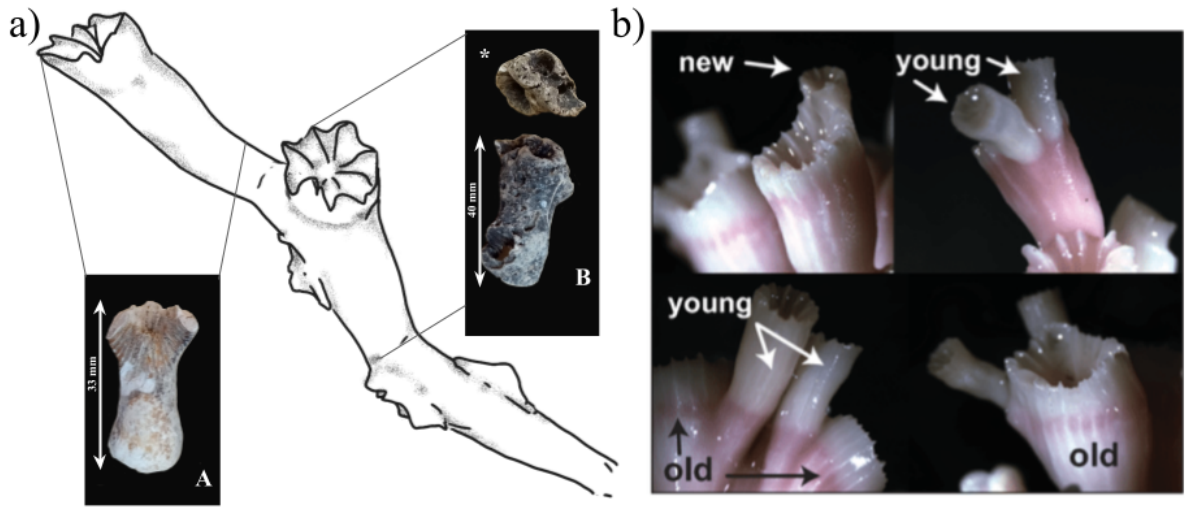

Figure 12 - a) Position of each fragment within branches of *Lophelia pertusa* specimen. Illustration made by the author; b) Photographs of live *Lophelia pertusa* polyps in different life stages.
Source: Illustration by the author. Photograph by MAIER *et al.* (92)

Mh also presents a bifurcation growing pattern, resulting from budding of polyps. This pattern is evident in Figure 13 - b. Which also shows heterogeneous distribution of porous regions. The area highlighted by the white square is used in further discussion.

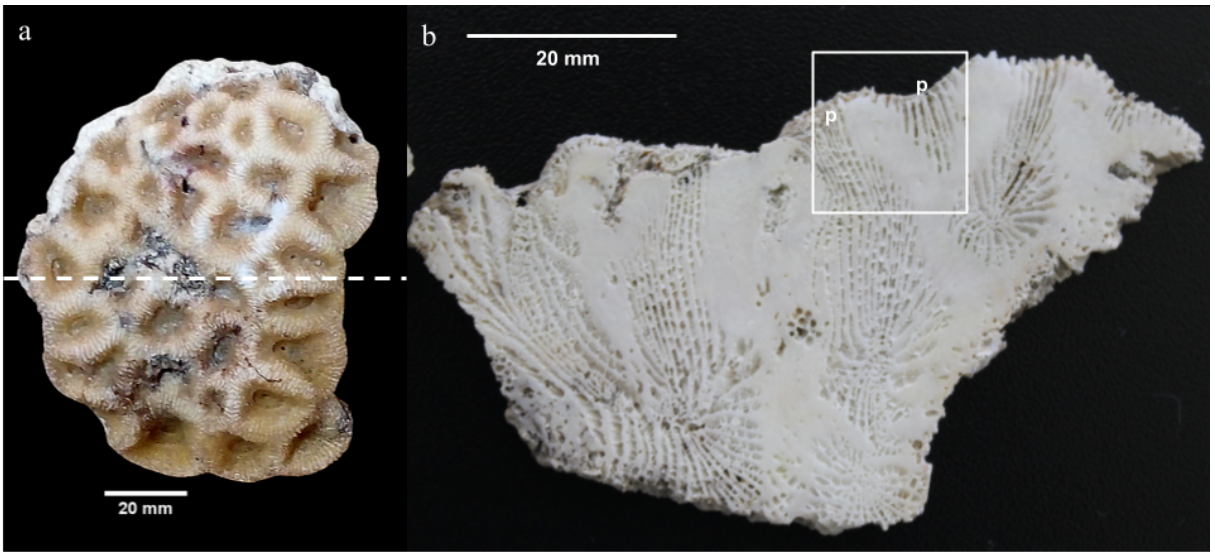

Figure 13 - a) Mh sample with cut location; b) transversal section of Mh.
Source: By the author.

4.3 Chemical composition

Considering the presented literature, the coral skeletons are expected to be calcium carbonate that can be confirmed by energy dispersive spectroscopy. The following Table 6 shows averaged results for *Mh*, *Lp*A and *Lp*B.

Qualitatively, the composition is calcium carbonate, as the most abundant elements found are Calcium, Carbon and Oxygen. For all the samples, the sum of O, Ca and C fraction already sums more than 99 at%.There are trace elements that can be found as ions in seawater and are commonly present in inorganic tissues of biological origin.

Table 6 - EDS results for each sample.

	Mh		*Lp*A		*Lp*B	
Elements	at%	σ	at%	σ	at%	σ
O	55.1	0.8	58.2	0.9	54	1
Ca	14.8	0.3	18.1	0.3	14.2	0.5

(continued)

(continuation)

Table 6 - EDS results for each sample.

	Mh		*Lp*A		*Lp*B	
Elements	at%	σ	at%	σ	at%	σ
C	29.7	0.9	24	1	31	1
Al	-	-	-	-	0.08	0.02
Cl	-	-	-	-	0.30	0.04
Mg	0.02	0.01	0.12	0.1	0.08	0.06
Na	0.19	0.08	0.18	0.09	0.15	0.06
S	0.08	0.06	-	-	-	-
Si	-	-	0.19	0.04	-	-
Sr	0.18	0.04	0.13	0.03	0.11	0.04

Source: By the author.

4.4 Crystal structure

Crystal structure comprises the results of XRD analysis. Both skeletal samples were identified as aragonite due to their diffractogram patterns and peak positions. This will be further disclosed in this section as Rietveld refinement results are presented. Figure 14 shows the measured patterns for all samples, normalized to 100 by intensity of (111) peak at 26º. According to RRUFF database (RRUFF ID R080142) (95) the corresponding microstructure (upper organization of crystals) of samples with the observed XRD pattern is acicular aragonite, referring to bundles or clusters of calcium carbonate from where needle-shaped crystals grow.

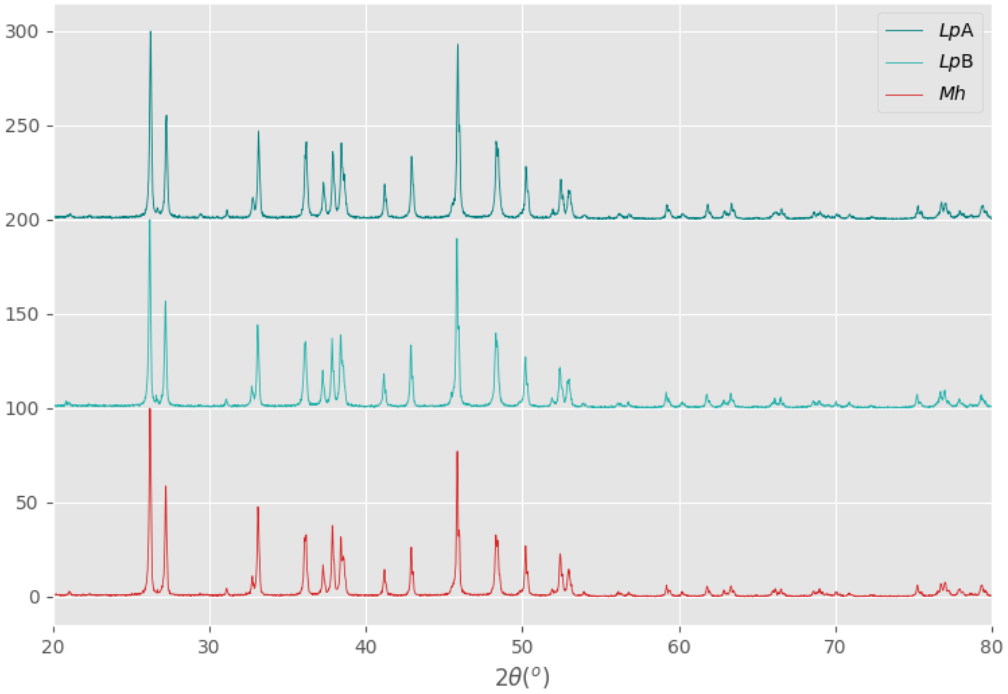

Figure 14 - X-ray diffractograms measured for both species, peaks normalized to 100.

Source: By the author.

Table 7 shows the lattice parameters for *Mh* and *Lp* obtained by Rietveld refinement. Literature reference of other two coral species, *Desmophyllum pertusum* (*Dp*) and *Favia stelligera* (*Fs*), by Stolarski *et al.* (96), will be shown in Table 8.

Rietveld refinement patterns are shown in Figure 15. The refinement presents a weighted residual (R_{wp}) of 15.33% for *Mh* and 20.67% for *Lp*. The ~5% difference between R_{wp} and R is provenient from the statistical weight derived from error propagation and is uncorrelated between data points of diffractogram. Samples are crystalline with average peak width of $0.14^{o} \pm 0.02^{o}$ for both *Mh* and *Lp*.

Table 7 - Rietveld refinement results according to GSAS II report.

	R_{wp}	R	a (Å)	b (Å)	c (Å)	V (Å^3)
Mh	15.33%	11.94%	4.96 ± 0.01	7.97 ± 0.02	5.75 ± 0.01	227.5
Lp	20.67%	16.48%	4.96 ± 0.03	7.97 ± 0.04	5.75 ± 0.03	227.3

Source: By the author.

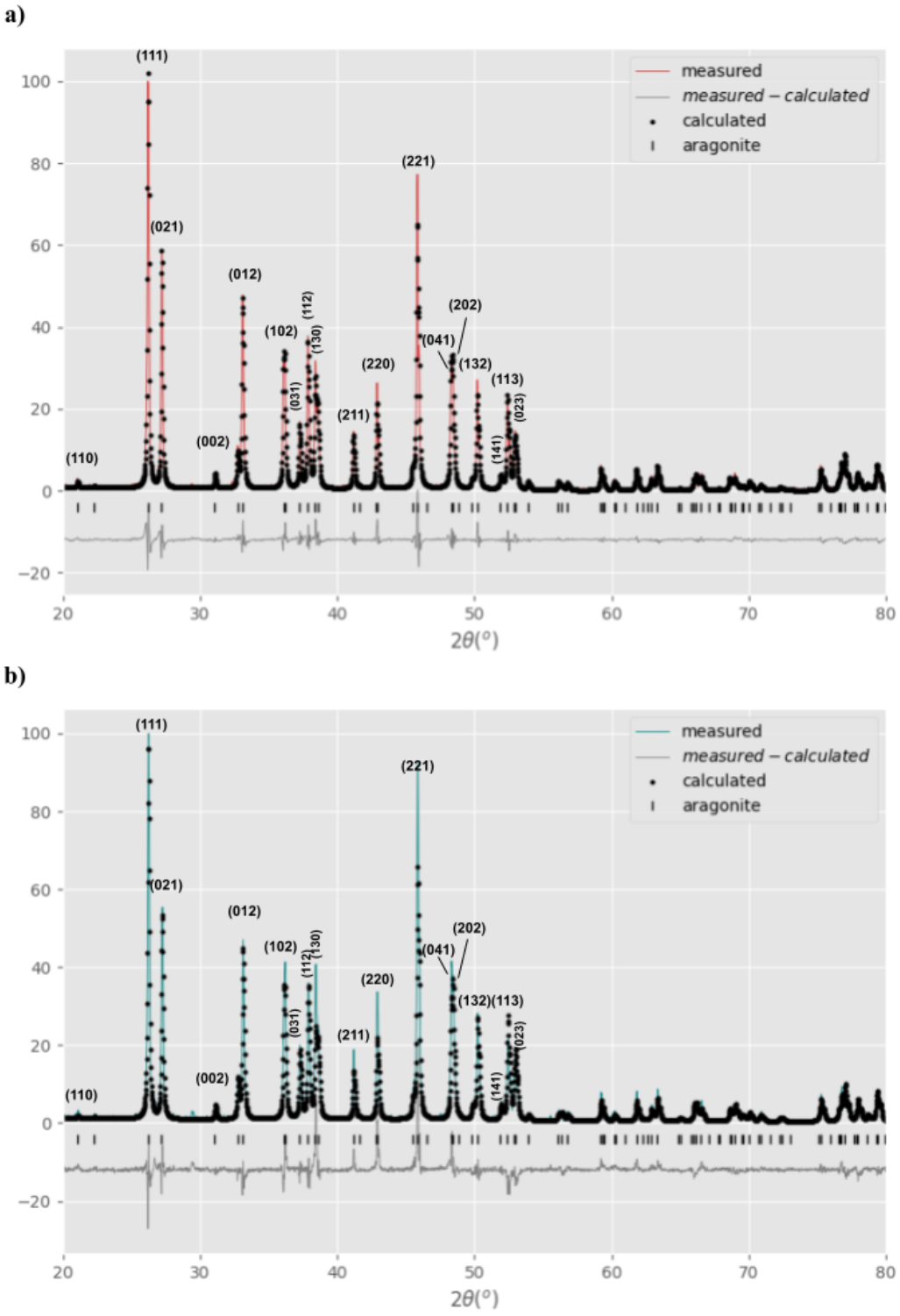

Figure 15 - measured X-ray diffractograms and refined patterns from Rietveld method. a) *Mh* and b) *Lp*.

Source: By the author.

Figure 16 shows 3D models of the refined structure's primitive cell obtained from refinement. The model accounts for lattice parameters but not for atomic radii as it would impair visualization.

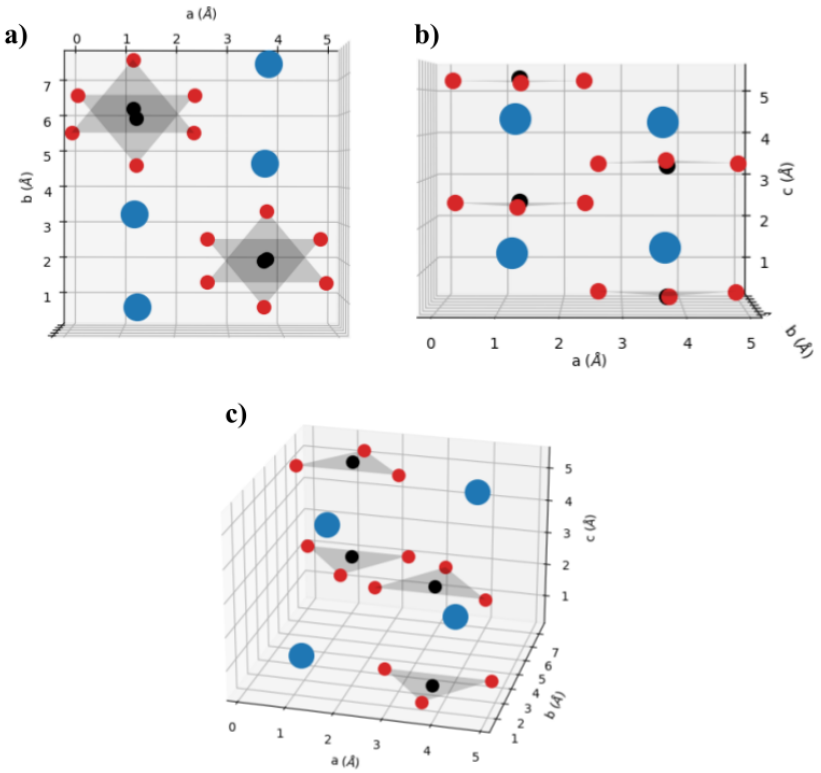

Figure 16 - 3D models of aragonite primitive cell. Calcium in blue, carbonates highlighted with gray planes. Source: By the author.

Reference refinements of biological aragonite, from Stolarski *et al.* (96) and geological aragonite, from Caspi *et al.* (35), are depicted in Figure 17 and Table 8. Both studies were conducted using synchrotron radiation with wavelength on tenths of Å (0.3 to 0.5 Å). The reference for biological aragonite is highly relevant for this work as it was conducted in corals from distinctive origins. *Dp* is a deep-water azooxanthellate coral, while *Fs* is a shallow-water zooxanthellate colonial coral.

The insets in Figure 17 a) and b) show the zoomed region of (102) and (200) peaks, used as standard for comparing aragonites of different origins, biological and geological. In geological aragonite peaks appear merged while are separated in biological aragonite. This condition is used as evidence to lattice distortions in b and c directions that are found in biological aragonite. These particular peaks have very similar values of interplanar spacing (d-spacing) and therefore are expected to appear close together. According to the refinement performed in *Mh* and *Lp* for the present dissertation, (102) and (200) have d-spacing values of 4.8755 and 4.8174 Å, respectively, leading to a 0.09 angular separation in the measured diffractogram between peak centers.

It is not possible to affirm that our samples present the expected lattice distortion due to experiment precision. Moreover, the lattice distortion claimed by several authors is normally found after the hundredths of Å, and percent differences in dimension range between 0.15% and 0.3%.

Table 8 - Rietveld refinement results according to reference.

	Residuals	a (Å)	b (Å)	c (Å)	V (Å^3)
Dp (96)	R_B= 35%	4.96499(5)	7.96992(8)	5.74892(8)	227.488(5)
Fs (96)	R_B= 8%	4.96509(2)	7.97226(3)	5.75004(2)	227.603(2)
Geological aragonite (35)	R_{wp} = 5.47%	4.96183(1)	7.96914(2)	5.74285(2)	227.081(1)

Source: compiled by the author.

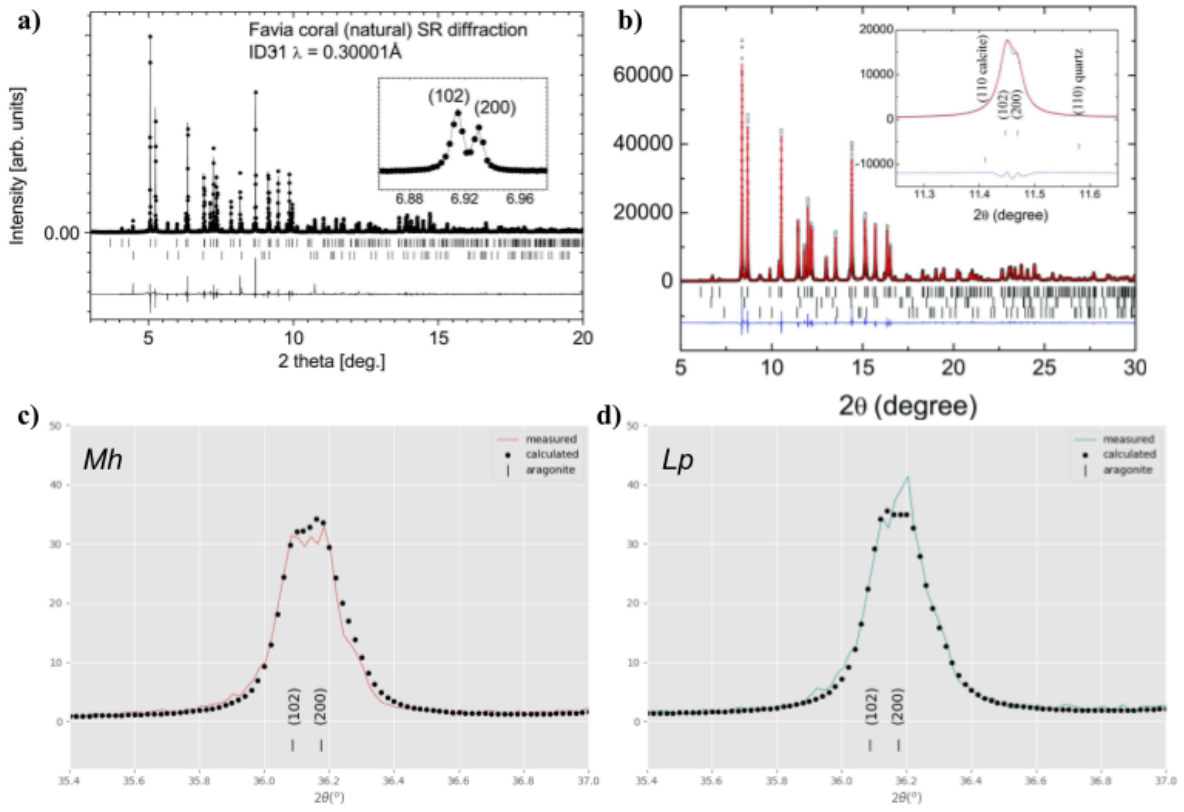

Figure 17 - a) Rietveld refined synchrotron radiation diffractogram of coral sample *Favia sp*; d) Rietveld refined synchrotron radiation diffractogram of geological aragonite. Peaks (102) and (200) shown in inset; c) and d) peaks (102) and (200) for *Mh* and *Lp*.
Source: Compiled by the author. Original image from STOLARSKI *et al.* (96); CASPI *et al.* (35).

Due to conditions of data collection, the reference refinements are considered highly reliable, however the presented refinement residuals are inconsistent. On one hand, Caspi *et al*. (35) do present the weighted residuals that are in comparable scale to this work's, but are not normalized to 100% as the standard returned by GSAS II. Value in Table 8 is corrected to facilitate comparison. On the other hand, Stolarski *et al*. (96) only shows Bragg factors as residuals which are not present in GSAS II reports and are a different statistical scale, but are shown as authors published in Table 8.

4.5 SEM analysis

SEM analysis in this study allows for identification of microstructure and morphology of crystalline superstructures, i.e., secondary organization of aragonite crystals beyond. As it has been proposed by Przeniosło *et al*. (45) and Mollica *et al.* (69), evidence of two-step crystal growth, RAD and TD, and extension and densification. Also, considering the age of *Lp*, diagenetic effects can also be identified in microstructure, as proposed by Hendy *et al.* (64) and Sayani *et al.* (62). And identification of growth fronts and mature skeletons like the ones shown in Figure 18.

When studying microstructure on coral skeletons, pores are especially interesting as they are formed due to soft tissue slotting and anchoring, leaving indentations as the coral grows further. Then, pores are the interface of live tissue and inorganic skeleton enclosed and isolated. Considering calcium carbonate formation starts as a biological process to later become an inorganic process of particle and ion attachments, (72) it is credible that the interface bears marks of deposition mechanisms and is likely to provide valuable information on biogenic aragonite growth.

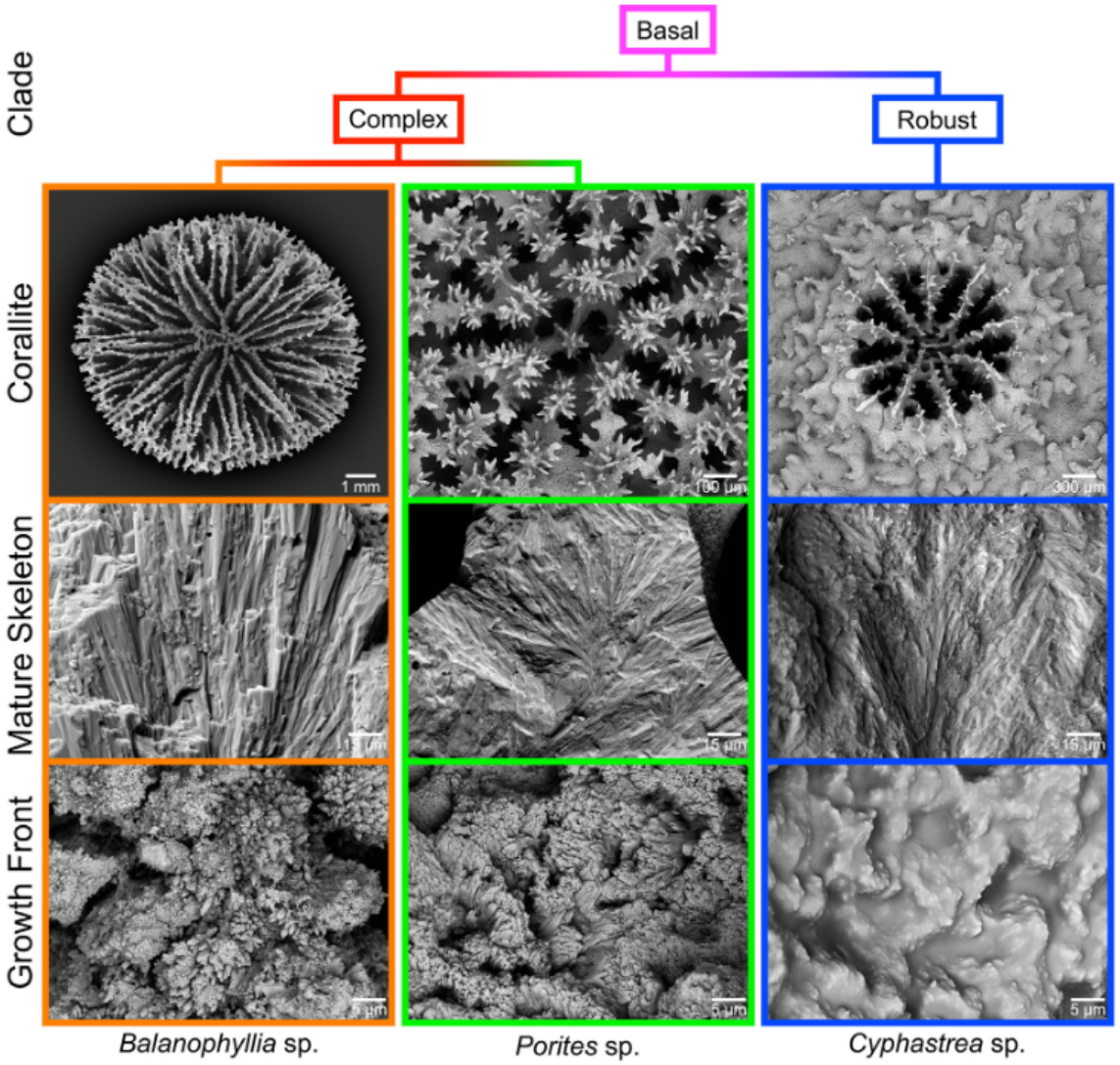

Figure 18 - SEM images of different coral species with different growth fronts and skeletal organizations.
Source: SUN *et al.* (71)

The SEM images on Figure 19 show different porous regions of *Mh*, a) and b) are not treated, while c) - f) were annealed at 200 ºC, below phase transition temperature to remove organic matter. White squares on the left column images represent the area analyzed on the right column. White arrows indicate important micro elements: flattened needles and spherulites. It is noteworthy that the three regions are different, as Figure 19 - a) presents deeper pores still covered in organic matter and its zoomed region, Figure 19 - b) presents flattened needles in a tight bundle. Figure 19 - c) with shallower pores and small particles aggregated at the bottom, in the zoomed portion of c) while showing the aggregates, some flattened needles can be seen below them. Finally, in Figure 19 - e) and f), even shallower pores and the zoomed region shows a tangled structure of needles amongst smaller particles.

The star-shaped formation to the right of the image is a probable precursor to the tangled threads. These images are likely to exemplify a progression of crystal growth, as the star-shaped formations precede the stage in f), that precedes d), that precedes b).

The star-like formation is also visible in the pores in Figure 18 - a) attached to the soft membrane that still covers the pores, inferring that they were biologically synthesized or formed at the ECF (72) and exported to be incorporated into the skeleton. Considering that *Mh* in particular was collected live and immediately placed in alcohol, it is plausible that ongoing metabolic processes were halted at any given stage. Moreover, pores and closed cavities of coral skeletons act as microenvironments, protecting its interior from solvents and external agents, allowing for an intact interior.

Insights on crystal growth are also provided by Figure 20 in which the aforementioned spiculated surface is present and would tell of aragonite dissolution and formation of secondary cement. Instead, this work proposes that, in the present case, the spiculated internal surface of the cavity in Figure 20 - a) and b) evidences crystal growth unrelated to deposition. The presence of a spherulite, a calcification center or precursor of aragonite needles, inside the cavity is a strong indicator of further calcification even without traces of organic matter. It is plausible that crystallites were seeded and could grow even after coral's body evacuated the pore vicinity.

This proposition can be reinforced by Figure 20 - c) and d) in which aragonite bundles, pointed by red arrows, fan out towards the center of a pore, also recovered in spiculated aragonite fabric. As these bundles grew, there would eventually be a bridge between the pore walls as exemplified by the sept in the red square. Another possibility would be the continuous growth of the whole spiculated surface that would eventually fill the pore space and form a solid region. Regardless of the outcome, the coral would benefit from the additional strength offered from further calcification of older structures.

Considering the biomineralization model by Sun *et al*. (73), and references within, the combination of particle and ion attachments form the skeleton. According to SUN *et al.* (73) uniform particles of calcium carbonate aggregate quickly, at 40 μm/day rate, mediated by biogenic processes, then coral skeleton is thickened by ion attachment at average 0.05 μm/day. The combined process also

The SEM images in this study show the formation of a primary scaffold of highly ordered microstructures, i.e., needles and aggregated needles, to which scattered particles and small crystallites join to. Considering Figure 12, the solid region inserted

between porous regions, indicated by **p**, might be formed after biologically induced calcification has terminated.

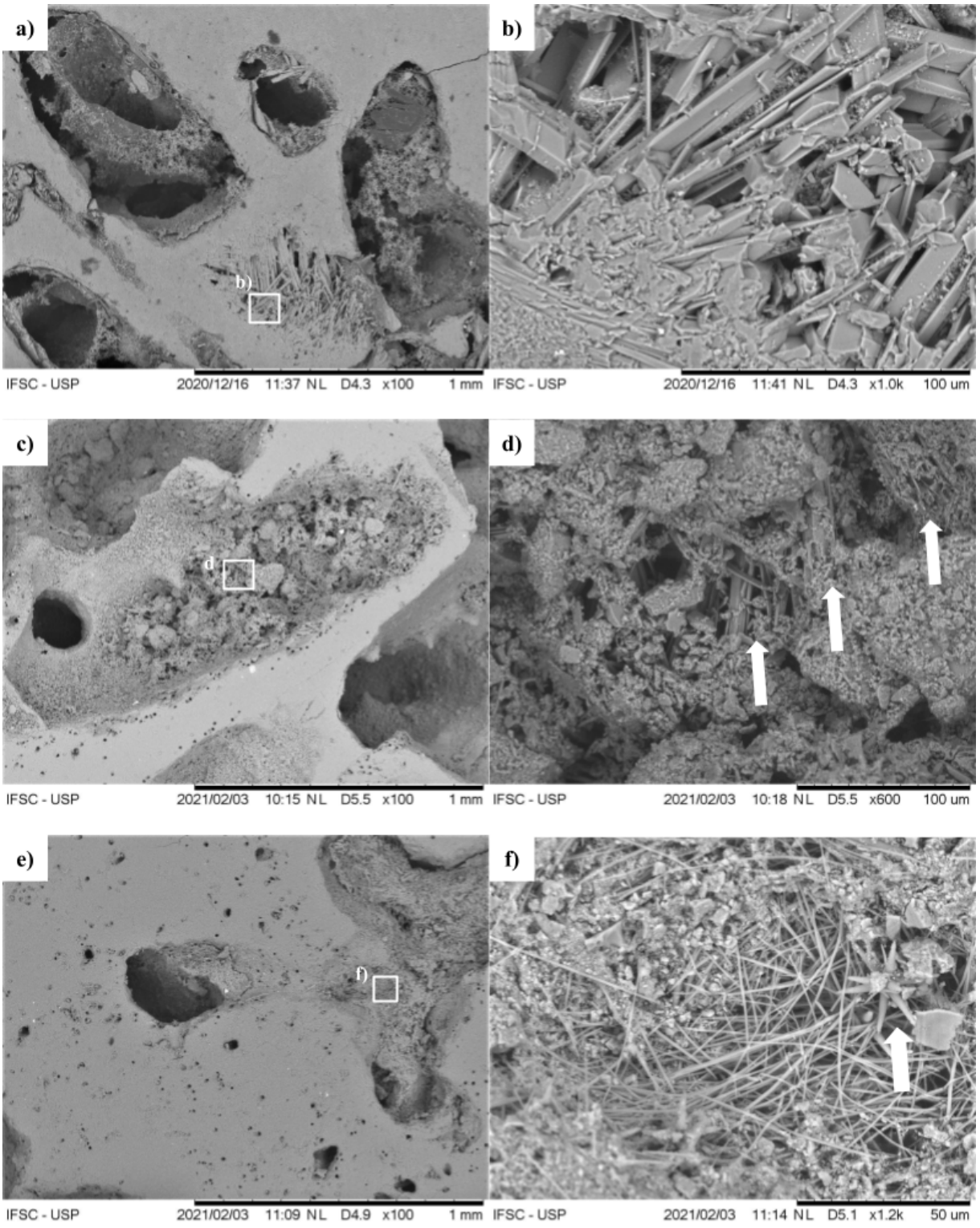

Figure 19 - SEM images of a) and b) non-treated sample; c) and d) 200 ºC thermally-treated sample; e) and f) 200 ºC thermally-treated.

Source: By the author.

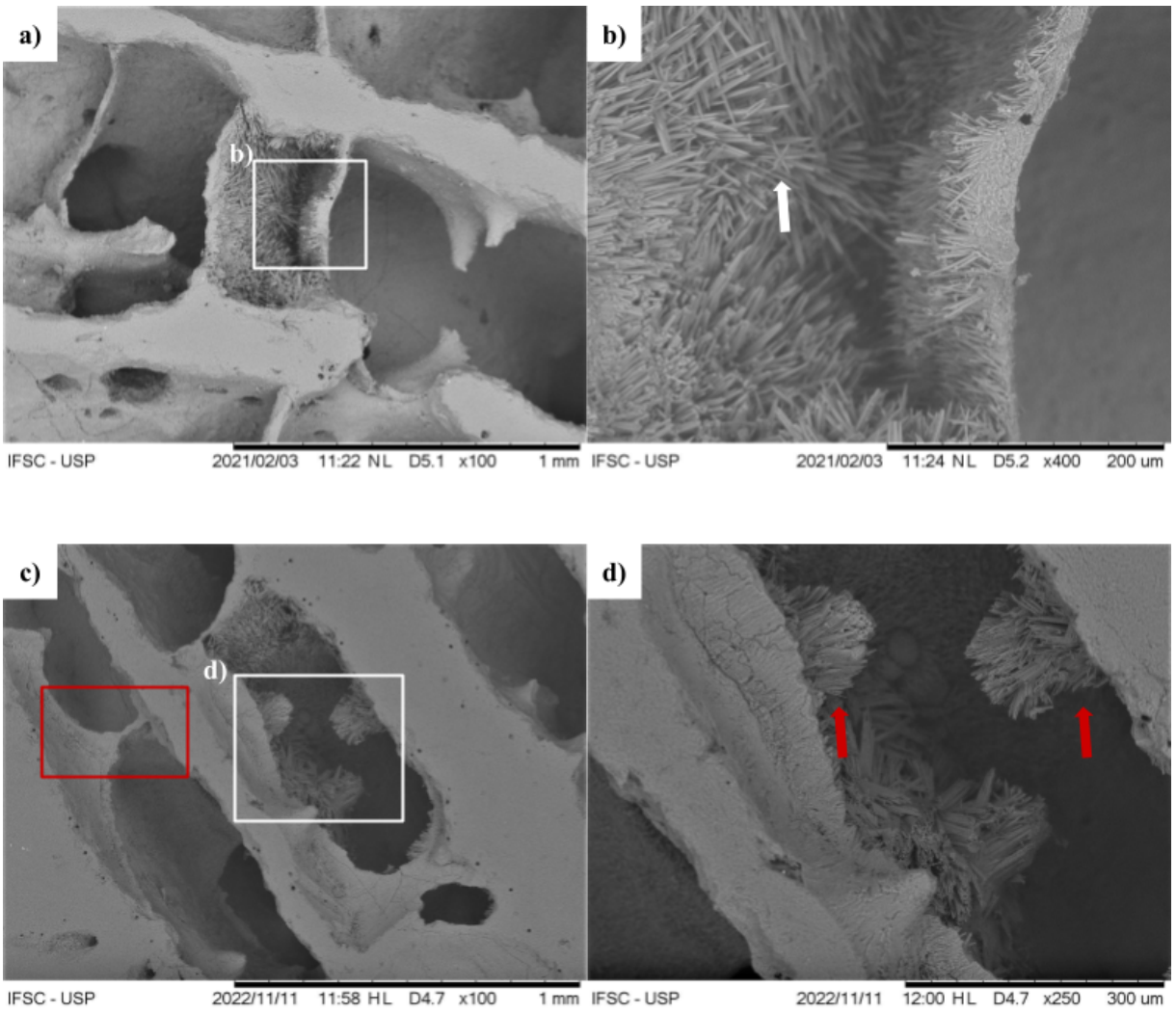

Figure 20 - SEM images of spiculated surfaces: a) sample treated at 200 ºC, white encircled area reference zoomed region in b); c) sample treated at 260 ºC, below the phase transition temperature, d) is a zoomed region of c).

Source: By the author.

Now considering *Lp* samples and substitution of the primary phase. We saw that the skeleton is in fact aragonite and the non-treated sample does not present trace calcite according to refinement. Then, if the primary aragonite was substituted, it was substituted by a secondary aragonite cement. The same approach of studying porous regions could not be done due to differences on calcification fronts and porosity: *Lophelia pertusa* is considerably less porous.

Figure 21 does not show pores, but imperfections on skeleton that reveal microstructure and microstructure, shows a spiculated surface much different from the ones seen in Figure 20 - b), considering spicules size and integrity. Already discussed in previous sections, the fragment *Lp*B burned appearance is most probably related to exposure to sulfuric

acid in soil, thus causing surface etching. But it must be taken into account that the prolonged exposure to a strong acid would degrade the remaining skeleton and greatly impact structure.

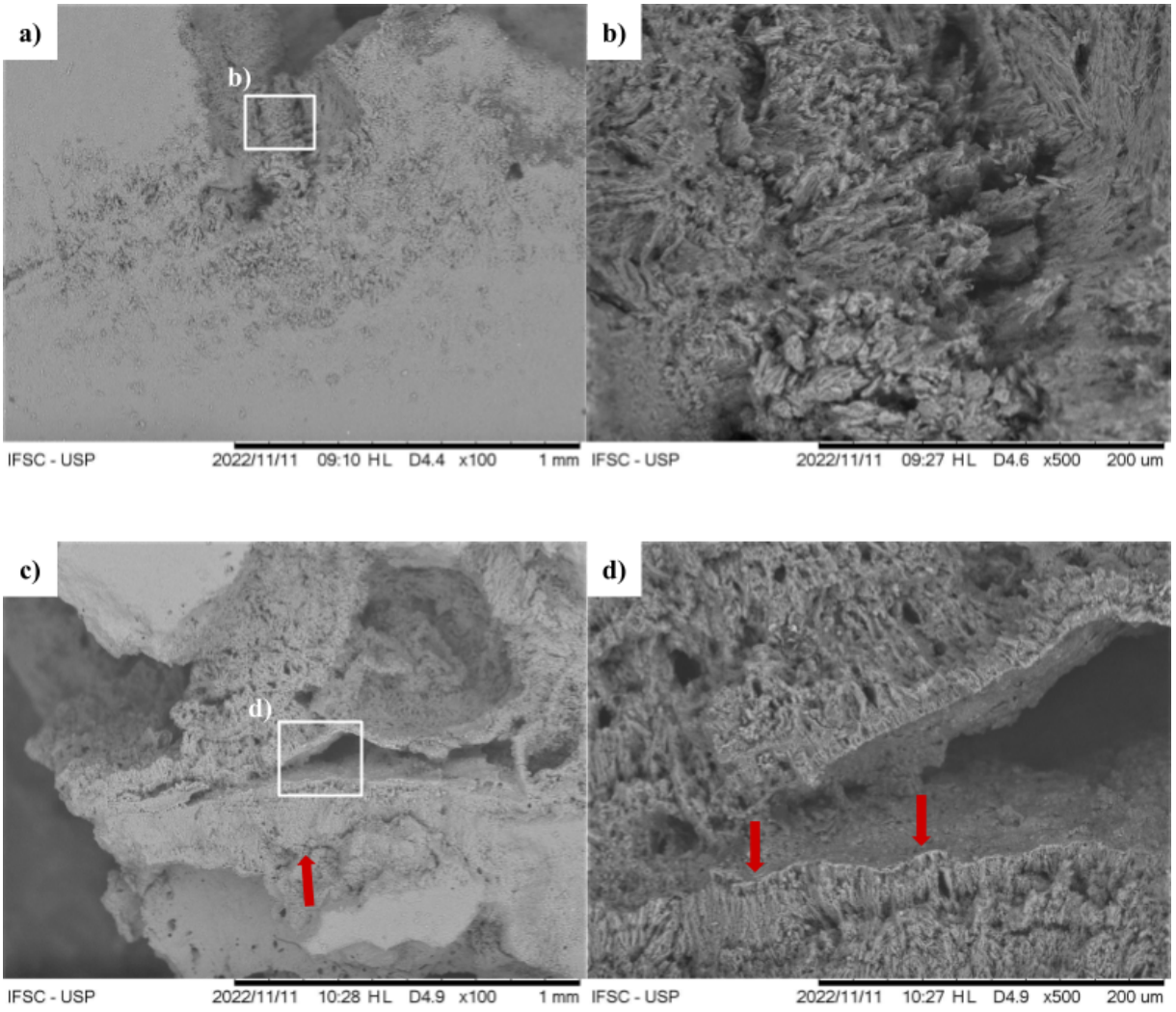

Figure 21 - SEM images of fragment *Lp*B, a) non-treated sample showing cut surface to reveal flattened needles and small grains in skeletal growth scar; b) zoomed region of a) shows fan-like formations of aragonite stemming from a calcification center; c) sample treated at 260 ºC, showing porous region with preserved microstructure; d) zoomed region of c), in which is visible mature skeleton, highlighted by red arrows. Mature skeleton is organized in a fan of flattened needles.
Source: By the author.

Figure 22 presents etched surfaces of *Mh* sample that have been etched by a citric acid for 30 min and 60 min, a) and b) respectively. The 30 min chemical attack is capable of degrading the first layer of pristine aragonite while the 60 min attack shows signs of degrading the spiculated microstructure. By comparison, *Lp*B's surface does not present as much degradation as Figure 18 - b) exemplifies.

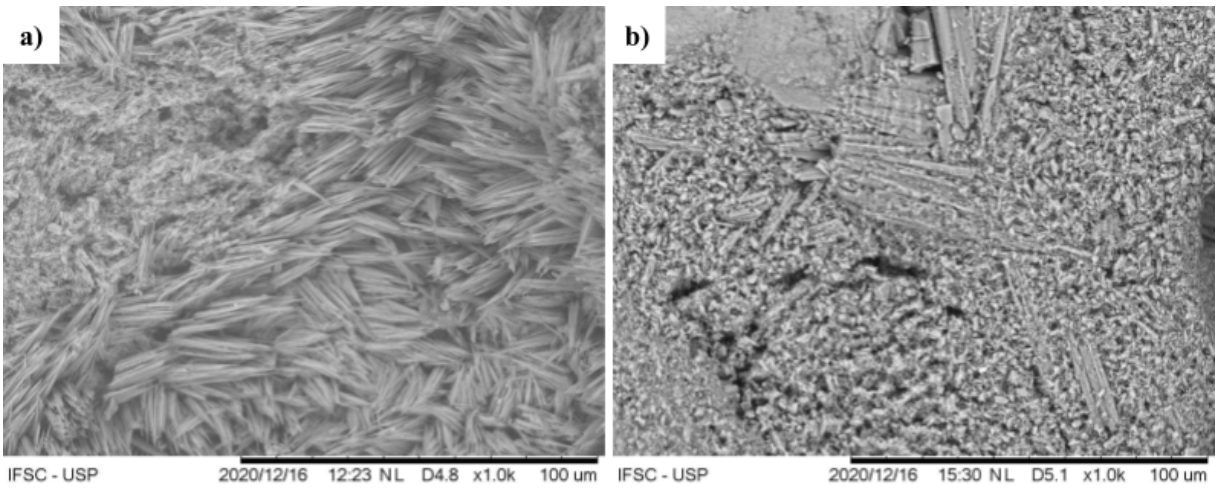

Figure 22 - Chemically etched *Mussismilia hispida* subsamples for a) 30 min, b) 60 min.
Source: By the author.

Figure 20 - c) and d) present a mature skeleton structure by comparison to SUN *et al.* (71), red arrows point at supporting structures. Skeleton has cracked and revealed aligned facies of aragonite flattened-needles, that relate to skeleton's growth model for *Lophelia pertusa*. Figure 23 where we see radial distributions of aragonite parting from the asterisk in the region framed in white.

Thus, the arrangement of acicular crystals visible might, alternatively, have been maintained through the years and *Lophelia pertusa*'s fragments were preserved in a stable environment with little contact with moisture, known to be closely related to diagenesis of aragonite sediments, supported by the absence of calcitic infiltrations despite sample's age. *Lp* fragments did maintain the sclereodermite microstructure proposed by Mouchi *et al*. (70).

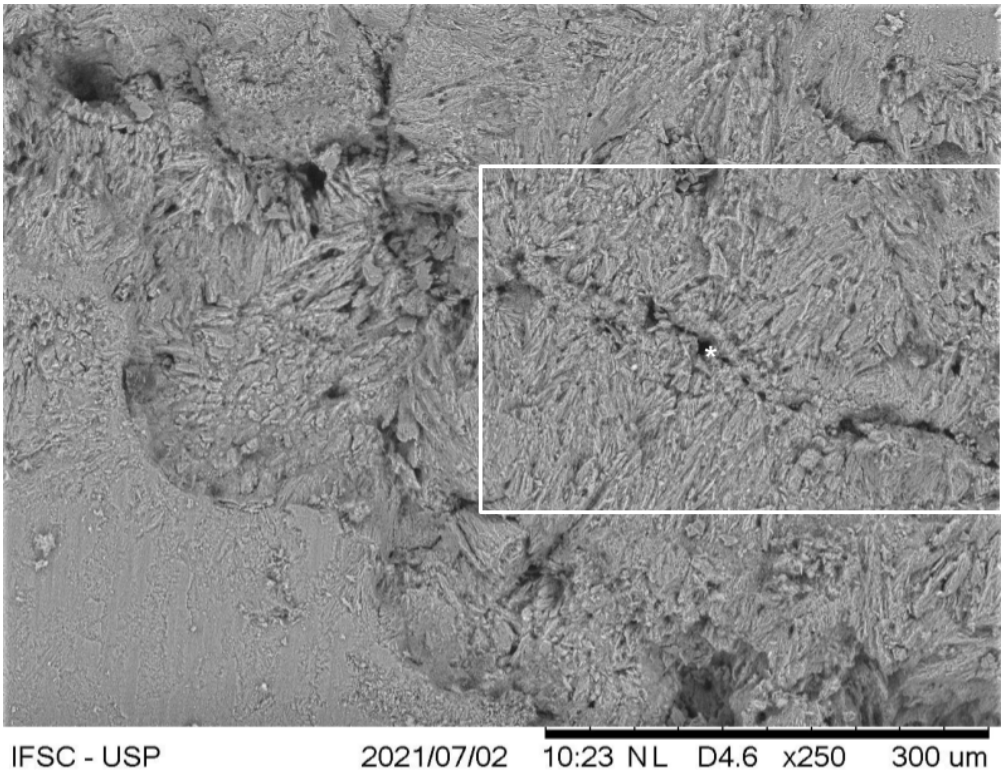

Figure 23 - SEM image of *Lp* surface. Emphasis on mature skeleton displayed by fan of flat aragonite needles and center or calcification, alternatively RAD, marked by asterisk.
Source: By the author.

4.6 Thermal behavior

When referring to sample behavior, this study's main focus is thermal stability of samples. As previously commented on, stability is a key criteria for all sorts of analysis of minerals and biogenic materials. When faced with *Lp* age, we might wonder if stability is maintained through long periods of time or even if both species will behave the same when heated.

First addressing the common mass loss between the two samples on step 2 above the temperature marked with a star (*), 547 ^{o}C, in Figure 24. Above this temperature, the vaporization of carbonate $(CO_3)^{-2}$ is expected, this process leads to the release of CO_2 below the explicit reaction:

$$CaCO_3 \Rightarrow CaO + CO_2$$

This vaporization is supposed to decrease sample mass by 44%, we effectively see for *Mh* and *Lp* a respective decrease of 41.15% and 39.85%. For this calculation, the mass loss of step 1 will be disregarded, and theoretical values for mass loss between 560 and 750 ^{o}C will be presented considering the starting mass of step 3 the full mass of the inorganic

phase. This is supported by the fact that no mineral phases are vaporized before the experiment reaches 550 ºC. (47–50) The starting mass fraction in step 2 is, for *Mh* and *Lp* in this order, 95.85% and 94.88%. This leads to theoretical values of 42.27% and 41.84%, respectively, which are equivalent to the experimental values.

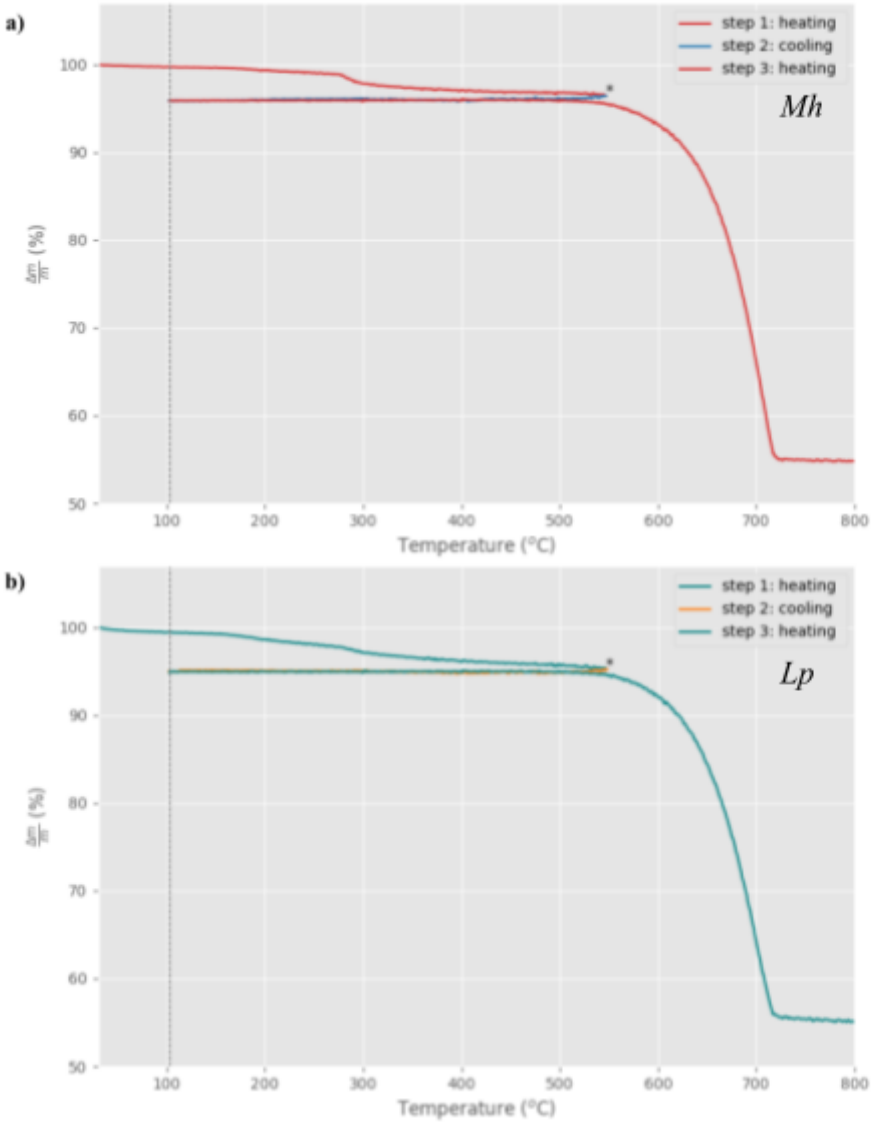

Figure 24 - Two step TG analysis for a) *Mh*, b) *Lp*.

Source: By the author.

The step 2 profile, then, indicates that changes observed in the first step are not reversible. An auxiliary XRD analysis was performed after heating samples above 550 ºC, and returned that samples have been fully transformed to calcite. Although expected, because aragonite from almost all sources face a phase transition around 400 - 450 ºC. (10)

Step 1 of TG is in Figure 25. Data demonstrates that samples present a slightly different behavior, although both samples present this constant mass decrease in the temperature interval.

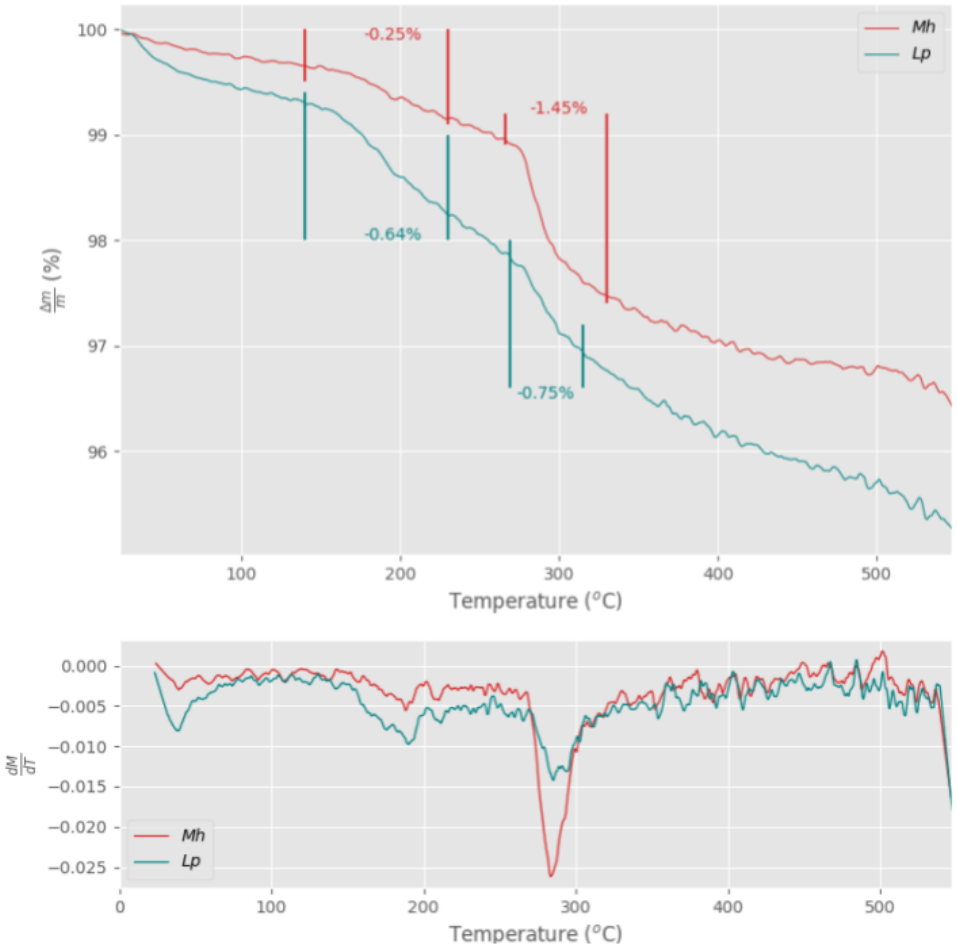

Figure 25 - Compared step 1 TG for Mh and Lp.

Source: By the author.

Between 160 ºC and 210 ºC, *Mh* and *Lp*, lose 0.25% and 0.64% respectively. This temperature is very much likely responsible for the vaporization of organic matter trapped in between crystallites. Next, samples show another event of mass loss, with *Mh* presenting signs of it around 5 ºC before *Lp*. This event is marked by a significantly larger mass loss from *Mh* when compared to *Lp*, explicit in Figure 23, marked by 1.45% versus 0.75%. The overall change for samples up to 540 ºC is 3.54% and 4.73%.

This is the temperature interval in which organic matter and water evaporate. The main references for this phenomena in this work proposed this mass loss to be water vapor. The water was previously in the sample as structural/interstitial water. (47–50)

When manipulating samples, one can notice that *Lp* is softer and chalkier than *Mh*, and the steeper event observed for *Mh* between 260 ºC and 330 ºC can be related to slower diffusion of molecules in between crystals that take a longer time to reach the surface due *Mh* being a less dissolved sample. But *Lp* still presents greater mass loss during heating.

Phase transition starting temperatures found for our samples align with the one cited by Okumura *et al.* (10): phase transition for coral aragonite starts at 280 ºC and ends at 440 ºC. *Mh* and *Lp*, however, show that the phase transition ends before 400 ºC, estimated at 310 ºC. The species used to assess the phase transition is *Galaxea fascicularis* that occurs between the east coast of Africa and all the way to the west coast of Asia and Oceania. (97) KOGA and NISHIKAWA (50) also report that the phase transition of coral aragonite, *Pavona sp.*, starts between 250 - 300 ºC and ends between 400 - 450 ºC according to XRD results parallel to heating.

A hypothesis for the difference between the observed phase transition temperatures is the different clades to which the species belong. Both *M. hispida* and *L. pertusa* stem from the Robusta clade, while both *G. fascicularis* and *Pavona sp.* stem from the Complexa clade, which gives these coral a fundamental genetic difference. (11,98) Skeletal comparison based on clade can be seen in Figure 18.

According to the XRD patterns in Figure 26 and the refinement results in Table 9 there is a progression of phase transition in respect to temperature. There is a difference in transformation rate tied to species that is shown by the calcitic phase fraction on *Mh* and *Lp*. Referring to Table 9, at 285 ºC, samples present different fractions of calcite mixed in aragonite.

Table 9 - GSAS II Rietveld refinement result report for samples treated at 285 ºC.

	R_{wp}(%)	phase	phase fraction	a (Å)	b (Å)	c (Å)	V (Å^3)
Mh	16.30	aragonite	0.748	4.96±0.01	7.97±0.02	5.75±0.01	227.5±0.03
		calcite	0.252	4.98±0.03	4.98±0.03	17.08±0.01	367.42±0.03
Lp	16.80	aragonite	0.912	4.96±0.03	7.97±0.04	5.75 ±0.03	227.3±0.01
		calcite	0.088	4.98±0.03	4.98±0.03	17.09±0.01	367.71±0.05

Source: By the author.

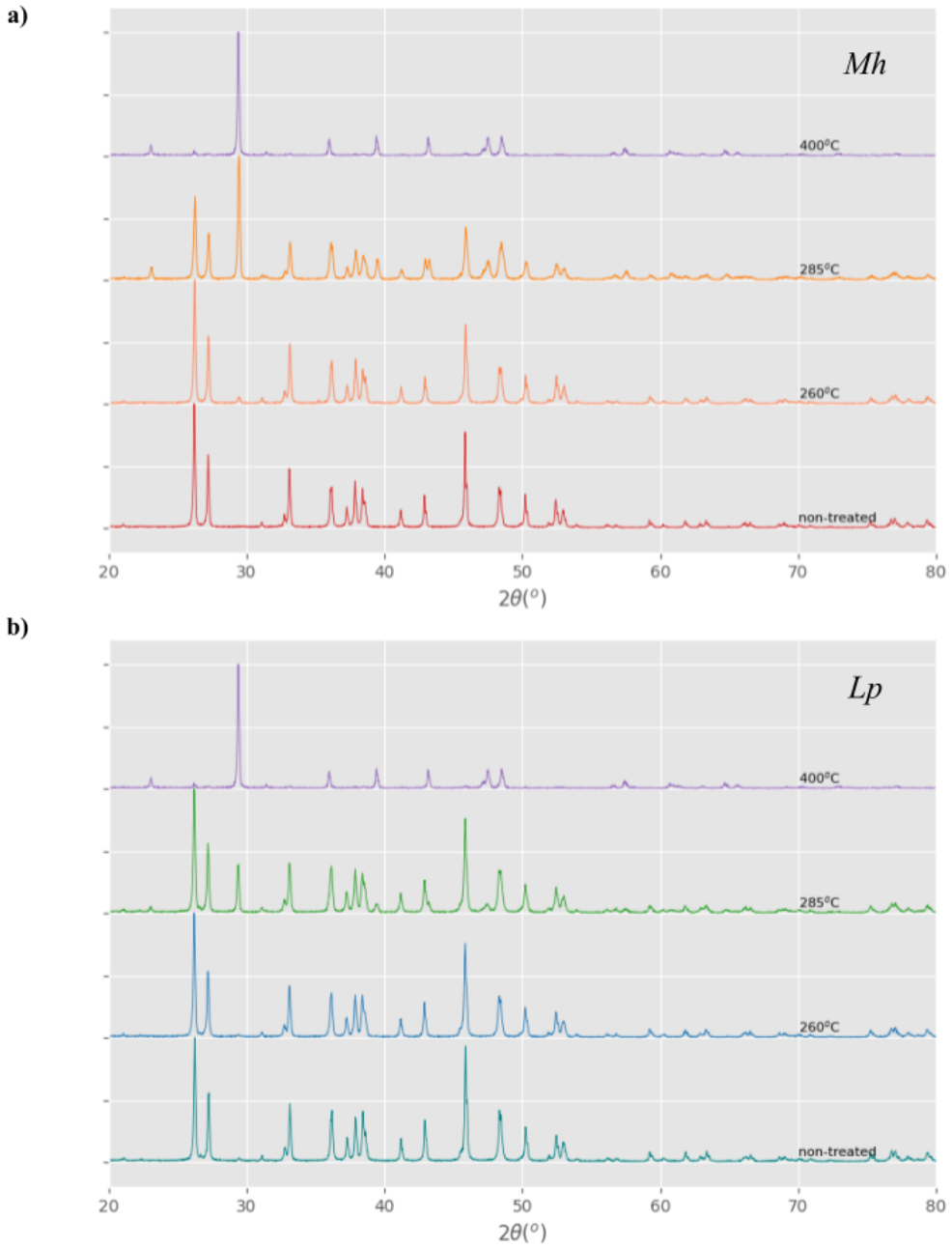

Figure 26 - X-ray diffractograms for varied temperatures, a) *Mh* and b) *Lp*. Diffectograms tell the sample's crystalline structure at selected temperatures to show the progression of phase transition: at 260 ºC sample is still aragonite, at 285 ºC sample has a fraction of both aragonite and calcite, at 400 ºC sample has fully transformed into calcite.

Source: By the author.

5 CONCLUSIONS

We saw that aragonites from different coral species of the brazilian fauna can present the same characteristics, such as crystalline structure, chemical composition and phase transitions. Both *Mh* and *Lp* have shown to be fully calcium carbonate, and then aragonite upon further analysis, while at room temperature and standard pressure. All these results could be compared and validated by fitting literature.

The radiocarbon dating revealed a very young material, *Mh*, and a very old material, *Lp*. The latter is categorized as being from the Upper-Pleistocene epoch around ~11700 years ago. SEM images could show that diagenetic effects that would be expected to affect *Lp* were not so present and primary deposits seem to be preserved. It is possible to identify signs of skeletal growth in *Mh* by the presence of spherulites and spherulites with elongated radii that are tangled in the organic matter.

Phase transition temperatures, however, did not fully compare to works available, as our samples have shown to end the phase transition at temperatures lower than expected. The main hypothesis for explaining this result connects to particularities of species, more precisely genetic differences between corals of different clades. The phenomena behind the different phase transition behavior has yet to be understood and can be explored further in future works.

The interpretation of this collection of data leads to the proposition and complementation of a growth mechanism for coral skeletons mainly approached in the structure section. SEM images evidenced the continuation of skeletal growth after the coral body has left the vicinity, and that particles aggregate around a scaffold of elongated aragonite needles and close the surface, leading to the 100% occupancy of aragonite. This model is aligned with what was previously proposed by other works, seeing that a primary structure is formed before a recruitment of particles.

5.1 Project limitations

The main limitation of this research project is the sample availability. Both from diversity, as it would enrich the project to explore more than two species and also *Lophelia pertusa* dimensions that limited the number of experiments that could be performed. Also some experiments, such as compressive strength, could not be performed due to sample dimensions and extension of porous regions.

5.2 Future directions

This project can be improved by diversifying the coral collection studied. From a material's science perspective, this project benefits from tackling phase transitions and its relation to species and skeletal microstructure. Amorphous calcium carbonate should be quantified alongside the other phases, as it is expected to be a precursor for skeleton formation. Other skeletons

The project's future directions lean towards the establishment of a biomineralization model, how corals control the steps of inorganic material deposition and how refined is this control. One of the goals being able to crystalize proteins involved in the process and elucidate its structure. Finally, how changing environments might affect reefs and reef builders from now on.

REFERENCES

1 CALLISTER, W. D.; RETHWISCH, D. G. **Materials science and engineering**: an introduction. 8th ed. Hoboken: John Wiley & Sons, 2010. 885 p. ISBN 978-0-470-41997-7.

2 DENG, Z.; JIA, Z.; LI, L. Biomineralized materials as model systems for structural composites: intracrystalline structural features and their strengthening and toughening mechanisms. **Advanced Science,** v. 9, n. 14, p. 2103524, 2022. ISSN 2198-3844. DOI: 10.1002/advs.202103524.

3 FU, K.; XU, Q.; CZERNUSZKA, J.; TRIFFITT, J. T.; XIA, Z. Characterization of a biodegradable coralline hydroxyapatite/calcium carbonate composite and its clinical implementation. **Biomedical Materials**, v. 8, n. 6, p. 065007, Nov. 2013. ISSN 1748-6041, 1748-605X. DOI 10.1088/1748-6041/8/6/065007.

4 LYU, B. *et al.* Coral aggregate concrete: numerical description of physical, chemical and morphological properties of coral aggregate. **Cement and Concrete Composites**, v. 100, p. 25–34, July 2019. ISSN 0958-9465. DOI 10.1016/j.cemconcomp.2019.03.016.

5 ELLIFF, C. I.; SILVA, I. R. Coral reefs as the first line of defense: Shoreline protection in face of climate change. **Marine Environmental Research**, v. 127, p. 148–154, 1 June 2017. ISSN 0141-1136. DOI 10.1016/j.marenvres.2017.03.007.

6 WOODROFFE, C. D.; WEBSTER, J. M. Coral reefs and sea-level change. **Marine Geology**, v. 352, p. 248–267, June 2014. ISSN 0025-3227. DOI 10.1016/j.margeo.2013.12.006.

7 ROVERE, A.; ANTONIOLI, F.; BIANCHI, C. N. Fixed Biological Indicators. *In*: SHENNAN, I.; LONG, A. J.; HORTON, B. P. (ed.). **Handbook of sea-level research**. Chichester, West Sussex: John Wiley & Sons, 2015. p. 267–280. ISBN 978-1-118-45254-7.

8 CAMOIN, G. F.; WEBSTER, J. M. Coral reef response to Quaternary sea‐level and environmental changes: state of the science. **Sedimentology**, v. 62, n. 2, p. 401–428, Feb. 2015. ISSN 0037-0746, 1365-3091. DOI 10.1111/sed.12184.

9 POKROY, B.; FITCH, A. N.; LEE, P. L.; QUINTANA, J. P.; CASPI, E. N.; ZOLOTOYABKO, E. Anisotropic lattice distortions in the mollusk-made aragonite: a widespread phenomenon. **Journal of Structural Biology**, San Diego, v. 153, n. 2, p. 145–150, Feb. 2006. ISSN 1047-8477. DOI 10.1016/j.jsb.2005.10.009.

10 OKUMURA, T.; YOSHIMURA, M.; KOGURE, T.; ENDO, K.; KOGURE, T.; NAGASAWA, H. On the transition temperature to calcite and cell lengths for various biogenic aragonites. *In*: ENDO, K.; KOGURE, T.; NAGASAWA, H. (ed.). **Biomineralization**. Berlin: Springer, 2018. p. 3–10. ISBN 9789811310027. DOI 10.1007/978-981-13-1002-7_1.

11 KITAHARA, M. V.; CAIRNS, S. D.; STOLARSKI, J.; BLAIR, D.; MILLER, D. J. A comprehensive phylogenetic analysis of the Scleractinia (Cnidaria, Anthozoa) based on mitochondrial CO1 sequence data. **PLoS ONE**, [*s. l.*], v. 5, n. 7, p. e11490, 8 July 2010. ISSN 1932-6203. DOI 10.1371/journal.pone.0011490.

12 PECHENIK, J. A. The Cnidarians. *In*: PECHENIK, J. A. **Biology of the invertebrates**. 7th. ed. New York: McGraw-Hill Education, 2015. p. 122–133. ISBN 978-0-07-352418-4.

13 DRAKE, J. L.; MASS, T.; STOLARSKI, J.; VON EUW, S.; SCHOOTBRUGGE, B. VAN DE; FALKOWSKI, P. G. How corals made rocks through the ages. **Global Change Biology**, v. 26, n. 1, p. 31–53, 2020. ISSN 1365-2486. DOI 10.1111/gcb.14912.

14 BOURNE, G. C. The Anthozoa. *In*: LANKESTER, E. R. (ed). **A treatise on zoology**: part II: the prorifere and coelenterata**.** London: A. and C. Black, 1900. Cap. 6. p. 1–84. Available from: https://www.biodiversitylibrary.org/page/21119831. Accessible at: 26 Sept. 2022.

15 SOARES, M. *et al.* Brazilian marine animal forests: a new world to discover in the Southwestern Atlantic. *In*: ROSSI, S. *et al*. (ed.). **Marine animal forests.** Berlin: Springer, Oct. 2016. p. 1–38. ISBN 978-3-319-17001-5. DOI 10.1007/978-3-319-17001-5_51-1.

16 HOEKSEMA, B.W.; CAIRNS, S. **World List of Scleractinia:** mussismilia hispida verrill 1901. Available from: https://www.marinespecies.org/aphia.php?p=taxdetails&id=290423 on 2022-08-08. Accessible at: 8 Aug. 2022.

17 HOEKSEMA, B. W.; CAIRNS, S. **World List of Scleractinia**: lophelia pertusa linnaeus 1758**.** Available from: https://www.marinespecies.org/aphia.php?p=taxdetails&id=135161. Accessible at: 11 Aug. 2022.

18 DALY, M.; FAUTIN, D. G.; CAPPOLA, V. A. Systematics of the Hexacorallia (Cnidaria: Anthozoa). **Zoological Journal of the Linnean Society,** v. 139, n. 3, p. 419–437, Nov. 2003. ISSN 0024-4082. DOI: 10.1046/j.1096-3642.2003.00084.x.

19 MUSCATINE, L.; TAMBUTTE, E.; ALLEMAND, D. Morphology of coral desmocytes, cells that anchor the calicoblastic epithelium to the skeleton. **Coral Reefs**, v. 16, n. 4, p. 205–213, Apr. 1997. ISSN 1432-0975. DOI: 10.1007/s003380050075.

20 FAUTIN, D. G. Structural diversity, systematics, and evolution of cnidae. **Toxicon,** v. 54, n. 8, p. 1054–1064, Dec. 2009. ISSN 0041-0101. DOI: 10.1016/j.toxicon.2009.02.024.

21 PEIXOTO, R. S. *et al.* Coral probiotics: premise, promise, prospects. **Annual Review of Animal Biosciences**, v. 9, n. 1, p. 265–288, 2021. DOI: 10.1146/annurev-animal-090120-115444.

22 SCHUHMACHER, H.; ZIBROWIUS, H. What is hermatypic?: a redefinition of ecological groups in corals and other organisms. **Coral Reefs**, v. 4, n. 1, p. 1–9, Apr. 1985. ISSN 0722-4028, 1432-0975. DOI: 10.1007/BF00302198.

23 COHEN, I.; DUBINSKY, Z.; EREZ, J. Light enhanced calcification in hermatypic corals: new insights from light spectral responses. **Frontiers in Marine Science**, v. 2, 2016. ISSN 2296-7745. Available from: https://www.frontiersin.org/articles/10.3389/fmars.2015.00122. Accessible at: 9 Sept. 2022.

24 CHAPPELL, J. Coral morphology, diversity and reef growth. **Nature**, v. 286, n. 5770, p. 249–252, July 1980. ISSN 1476-4687. DOI: 10.1038/286249a0.

25 LEÃO, Z. M. A. N. *et al.* Brazilian coral reefs in a period of global change: a synthesis. **Brazilian Journal of Oceanography**, v. 64, p. 97–116, 2016. ISSN 1679-8759, 1982-436X. DOI 10.1590/S1679-875920160916064sp2.

26 STOLARSKI, J. *et al.* A modern scleractinian coral with a two-component calcite–aragonite skeleton. **Proceedings of the National Academy of Sciences**, v. 118, n. 3, p. e2013316117, Jan. 2021. ISSN 0027-8424, 1091-6490. DOI: 10.1073/pnas.2013316117.

27 GATTUSO, J. P.; FRANKIGNOULLE, M.; SMITH, S. V.; WARE, J. R.; WOLLAST, R. Coral reefs and carbon dioxide. **Science**, v. 271, n. 5253, p. 1298–1298, Mar. 1996. DOI: 10.1126/science.271.5253.1298-a.

28 CHESWORTH, W. **Encyclopedia of soil science**. Dordrecht, Netherlands: Springer, 2008. 902 p. ISBN 978-1-4020-3994-2.

29 UKITA, M.; TOYOURA, K.; NAKAMURA, A.; MATSUNAGA, K. Pressure-induced phase transition of calcite and aragonite: a first principles study. **Journal of Applied Physics**, v. 120, n. 14, p. 142118, Oct. 2016. ISSN 0021-8979, 1089-7550. DOI: 10.1063/1.4961723.

30 SPÖTL, C.; FOHLMEISTER, J.; CHENG, H.; BOCH, R. Modern aragonite formation at near-freezing conditions in an alpine cave, Carnic Alps, Austria. **Chemical Geology**, v. 435, p. 60–70, Oct. 2016. ISSN 00092541. DOI: 10.1016/j.chemgeo.2016.04.017.

31 FRISIA, S.; BORSATO, A.; FAIRCHILD, I. J.; MCDERMOTT, F.; SELMO, E. M. Aragonite-calcite relationships in speleothems (Grotte De Clamouse, France): environment, fabrics, and carbonate geochemistry. **Journal of Sedimentary Research**, v. 72, n. 5, p. 687–699, Sept. 2002. ISSN 1527-1404. DOI: 10.1306/020702720687.

32 DUAN, W.; CAI, B.; TAN, M.; LIU, H.; ZHANG, Y.. The growth mechanism of the aragonitic stalagmite laminae from Yunnan Xianren Cave, SW China revealed by cave monitoring. **Boreas**, v. 41, n. 1, p. 113–123, 2012. ISSN 1502-3885. DOI: 10.1111/j.1502-3885.2011.00226.x.

33 TAS, A. C. Aragonite coating solutions (ACS) based on artificial seawater. **Applied Surface Science**, v. 330, p. 262–269, Mar. 2015. ISSN 01694332. DOI: 10.1016/j.apsusc.2014.12.195.

34 ZENG, M. *et al.* Confinement generates single-crystal aragonite rods at room temperature. **Proceedings of the National Academy of Sciences**, v. 115, n. 30, p. 7670–7675, July 2018. DOI: 10.1073/pnas.1718926115.

35 CASPI, E. N.; POKROY1, B.; LEE, P. L.; QUINTANA, J. P.; ZOLOTOYABKO, E. On the structure of aragonite. **Acta Crystallographica Section B:** structural science, v. 61, n. 2, p. 129–132, 1 Apr. 2005. ISSN 0108-7681. DOI: 10.1107/S0108768105005240.

36 POKROY, B.; FIERAMOSCA, J. S.; VON DREELE, R. B.; FITCH, A. N.; CASPI, E. N.; ZOLOTOYABKO, E. Atomic structure of biogenic aragonite. **Chemistry of Materials**, v. 19, n. 13, p. 3244–3251, June 2007. ISSN 0897-4756. DOI: 10.1021/cm070187u.

37 OGILVIE, M. M. III. Microscopic and systematic study of madreporarian types of corals. **Philosophical Transactions of the Royal Society of London**, v. 187, p. 83–345, Dec. 1896. ISSN 0264-3960, 2053-9266. DOI: 10.1098/rstb.1896.0003.

38 WELLS, J. W.; STUMM, E. C.; HILL, D. Treatise on invertabrate paleontology: part F: Coelenterata. *In*: MOORE, R. C. (ed). **Treatise on invertabrate paleontology**. New York: University of Kansas Press, 1956. (Geological Society of America). p. 328–437. DOI: 10.17161/dt.v0i0.5539. Available from: https://journals.ku.edu/InvertebratePaleo/article/view/5539. Accessible at: 4 Oct. 2022.

39 BARNES, D. J.; DEVEREUX, M. J. Variations in skeletal architecture associated with density banding in the hard coral Porites. **Journal of Experimental Marine Biology and Ecology**, v. 121, n. 1, p. 37–54, Sept. 1988. ISSN 00220981. DOI:

10.1016/0022-0981(88)90022-6.

40 GOREAU, T. F. Calcium carbonate deposition by coralline algae and corals in relation to their roles as reef-builders. **Annals of the New York Academy of Sciences**, 1963. DOI: 10.1111/j.1749-6632.1963.tb13465.x.

41 KNUTSON, D. W.; BUDDEMEIER, R. W.; SMITH, S. V. Coral Chronometers: seasonal growth bands in reef corals. **Science**, v. 177, n. 4045, p. 270–272, 21 July 1972. DOI: 10.1126/science.177.4045.270.

42 GAFFEY, S. J.; KOLAK, J. J.; BRONNIMANN, C. E. Effects of drying, heating, annealing, and roasting on carbonate skeletal material, with geochemical and diagenetic implications. **Geochimica et Cosmochimica Acta**, v. 55, n. 6, p. 1627–1640, June 1991. ISSN 0016-7037. DOI: 10.1016/0016-7037(91)90134-Q.

43 CUIF, J-P.; DAUPHIN, Y.; DENIS, A.; GAUTRET, P.; KIYASHKO, S.; MASSAULT, M. Facteurs de la diagenèse précoce des biominéraux: exemple d'un polypier de Porites de Nouvelle-Calédonie. **Geobios**, v. 30, p. 171–179, Jan. 1997. ISSN 0016-6995. DOI: 10.1016/S0016-6995(97)80022-8.

44 STOLARSKI, J. Three-dimensional micro- and nanostructural characteristics of the scleractinian coral skeleton: A biocalcification proxy. **Acta Palaeontologica Polonica**, v. 48, p. 497–530, Nov. 2003.

45 PRZENIOSŁO, R.; STOLARSKI, J.; MAZUR, M.; BRUNELLI, M. Hierarchically structured scleractinian coral biocrystals. **Journal of Structural Biology**, v. 161, n. 1, p. 74–82, Jan. 2008. ISSN 1047-8477. DOI: 10.1016/j.jsb.2007.09.020.

46 OMER, M. *et al.* Structural and mechanical properties of staghorn coral (*Acropora cervicornis*) $CaCO_3$ aragonite skeletons, cleaned by chemical bleaching and biological processes. **Advances in Applied Ceramics**, v. 119, n. 8, p. 434–438, Nov. 2020. ISSN 1743-6753, 1743-6761. DOI: 10.1080/17436753.2020.1815500.

47 KIMURA, T.; KOGA, N. Monohydrocalcite in comparison with hydrated amorphous calcium carbonate: precipitation condition and thermal behavior. **Crystal Growth & Design**, v. 11, n. 9, p. 3877–3884, Sept. 2011. ISSN 1528-7483, 1528-7505. DOI: 10.1021/cg200412h.

48 kimura, t.; koga, n. thermal dehydration of monohydrocalcite: overall kinetics and physico-geometrical mechanisms. **Journal of Physical Chemistry A**, v. 115, n. 38, p. 10491–10501, Sept. 2011. ISSN 1089-5639, 1520-5215. DOI: 10.1021/jp206654n.

49 KOGA, N.; KASAHARA, D.; KIMURA, T. Aragonite crystal growth and solid-state aragonite–calcite transformation: a physico–geometrical relationship via thermal dehydration of included water. **Crystal Growth & Design**, v. 13, n. 5, p. 2238–2246, May 2013. ISSN 1528-7483. DOI: 10.1021/cg400350w.

50 KOGA, N.; NISHIKAWA, K. Mutual relationship between solid-state aragonite–calcite transformation and thermal dehydration of included water in coral aragonite. **Crystal Growth & Design**, v. 14, n. 2, p. 879–887, Feb. 2014. ISSN 1528-7483. DOI: 10.1021/cg4018689.

51 NEUMANN-MICHEAU, N.; TRIBUTSCH, H. Luminescence light collection technology in the aragonite of stone corals. **Bioinspiration & Biomimetics**, v. 13, n. 6, p. 066006, Oct. 2018. ISSN 1748-3190. DOI: 10.1088/1748-3190/aae1bf.

52 SWART, P. K. The strontium, magnesium and sodium composition of recent scleractinian coral skeletons as standards for palaeoenvironmental analysis. **Palaeogeography, Palaeoclimatology, Palaeoecology**, v. 34, p. 115–136, Jan. 1981. ISSN 0031-0182. DOI: 10.1016/0031-0182(81)90060-2.

53 CHALKER, B. E. Chapter 4: Skeletogenesis in scleractinian corals: the transport and deposition of strontium and calcium. *In*: SKORYNA, S. C. (ed.). **Handbook of stable strontium**. New York: Springer, 1981. ISBN 978-1-4684-3700-3.

54 SKORYNA, S. C. **Handbook of stable strontium**. New York: Springer US, 1981. ISBN 978-1-4684-3700-3. DOI: 10.1007/978-1-4684-3698-3. Available from: http://link.springer.com/10.1007/978-1-4684-3698-3. Accessible at: 18 Oct. 2022.

55 BECK, J. W. *et al.* Sea-surface temperature from coral skeletal strontium/calcium ratios. **Science**, v. 257, n. 5070, p. 644–647, 1992. ISSN 0036-8075.

56 GREEGOR, R. B.; PINGITORE, N. E.; LYTLE, F. W. Strontianite in coral skeletal aragonite. **Science**, v. 275, n. 5305, p. 1452–1454, Mar. 1997. ISSN 0036-8075, 1095-9203. DOI: 10.1126/science.275.5305.1452.

57 BRAHMI, C.; KOPP, C.; DOMART-COULON, I.; STOLARSKI, J.; MEIBOM, A. Skeletal growth dynamics linked to trace-element composition in the scleractinian coral Pocillopora damicornis. **Geochimica et Cosmochimica Acta**, v. 99, p. 146–158, Dec. 2012. ISSN 0016-7037. DOI: 10.1016/j.gca.2012.09.031.

58 SILVA, I. C. B. S. *et al.* Assessing the growth rate of the South Atlantic coral species Mussismilia hispida (Verrill, 1902) using carbon and oxygen stable isotopes. **Journal of South American Earth Sciences**, v. 96, p. 102346, Sept. 2019. ISSN 0895-9811. DOI: 10.1016/j.jsames.2019.102346.

59 FRIEDMAN, G. M. Early diagenesis and lithification in carbonate sediments. **Journal of Sedimentary Research**, v. 34, n. 4, p. 777–813, Dec. 1964. ISSN 1527-1404. DOI: 10.1306/74D71195-2B21-11D7-8648000102C1865D.

60 JONAS, L.; MÜLLER, T.; DOHMEN, R.; IMMENHAUSER, A.; PUTLITZ, B. Hydrothermal replacement of biogenic and abiogenic aragonite by Mg-carbonates – Relation between textural control on effective element fluxes and resulting carbonate phase. **Geochimica et Cosmochimica Acta**, v. 196, p. 289–306, 1 Jan. 2017. ISSN 0016-7037. DOI: 10.1016/j.gca.2016.09.034.

61 ALLISON, N.; FINCH, A. A.; WEBSTER, J. M.; CLAGUE, D. A. Palaeo environmental records from fossil corals: the effects of submarine diagenesis on temperature and climate estimates. **Geochimica et Cosmochimica Acta**, v. 71, n. 19, p. 4693–4703, Oct. 2007. ISSN 00167037. DOI: 10.1016/j.gca.2007.07.026.

62 SAYANI, Hussein R. *et al.* Effects of diagenesis on paleoclimate reconstructions from modern and young fossil corals. **Geochimica et Cosmochimica Acta**, [*s. l.*], v. 75, n. 21, p. 6361–6373, Nov. 2011. ISSN 00167037. DOI 10.1016/j.gca.2011.08.026.

63 MARTÍN-GARCÍA, R.; ALONSO-ZARZA, A. M.; MARTÍN-PÉREZ, A. Loss of primary texture and geochemical signatures in speleothems due to diagenesis: Evidences from Castañar Cave, Spain. **Sedimentary Geology**, v. 221, n. 1–4, p. 141–149, Nov. 2009. ISSN 00370738. DOI: 10.1016/j.sedgeo.2009.09.007.

64 HENDY, E. J.; GAGAN, M. K.; LOUGH, J. M.; MCCULLOCH, M.; DEMENOCAL, P. B. Impact of skeletal dissolution and secondary aragonite on trace element and isotopic climate proxies in *Porites* corals: diagenesis impacts on coral SST proxies. **Paleoceanography**, v. 22, n. 4, Dec. 2007. ISSN 08838305. DOI: 10.1029/2007PA001462.

65 NGUYEN, A. *et al.* Retaining geochemical signatures during aragonite-calcite transformation at hydrothermal conditions. **Minerals**, v. 11, n. 10, p. 1052, Sept. 2021. ISSN 2075-163X. DOI: 10.3390/min11101052.

66 JANISZEWSKA, Katarzyna; MAZUR, Maciej; MACHALSKI, Marcin; STOLARSKI, Jarosław. From pristine aragonite to blocky calcite: exceptional preservation and diagenesis of cephalopod nacre in porous Cretaceous limestones. **PLoS ONE**, v. 13, n. 12, p. e0208598, Dec. 2018. ISSN 1932-6203. DOI: 10.1371/journal.pone.0208598.

67 STOLARSKI, J.; MEIBOM, A.; PRZENIOSŁO, R.; MAZUR, M. A cretaceous scleractinian coral with a calcitic skeleton. **Science**, v. 318, n. 5847, p. 92–94, Oct. 2007. ISSN 0036-8075, 1095-9203. DOI: 10.1126/science.1149237.

68 CONCI, N.; VARGAS, S.; WÖRHEIDE, G. The biology and evolution of calcite and aragonite mineralization in Octocorallia. **Frontiers in Ecology and Evolution**, v. 9, 2021. ISSN 2296-701X. Available from: https://www.frontiersin.org/articles/10.3389/fevo.2021.623774. Accessible at: 9 Oct. 2022.

69 MOLLICA, N. R. *et al.* Ocean acidification affects coral growth by reducing skeletal density. **Proceedings of the National Academy of Sciences**, v. 115, n. 8, p. 1754–1759, Feb. 2018. ISSN 0027-8424, 1091-6490. DOI: 10.1073/pnas.1712806115.

70 MOUCHI, V.; VONLANTHEN, P.; VERRECCHIA, E. P.; CROWLEY, Q. G. Multi-scale crystallographic ordering in the cold-water coral Lophelia pertusa. **Scientific Reports**, v. 7, n. 1, p. 8987, Dec. 2017. ISSN 2045-2322. DOI: 10.1038/s41598-017-09344-5.

71 SUN, C-Y. *et al.* Crystal nucleation and growth of spherulites demonstrated by coral skeletons and phase-field simulations. **Acta Biomaterialia**, v. 120, p. 277–292, Jan. 2021. ISSN 1742-7061. DOI: 10.1016/j.actbio.2020.06.027.

72 GILBERT, P. U. P. A. *et al.* Biomineralization: integrating mechanism and evolutionary history. **Science Advances**, v. 8, n. 10, Mar. 2022. ISSN 2375-2548. DOI: 10.1126/sciadv.abl9653. Available from: https://www.science.org/doi/10.1126/sciadv.abl9653. Accessible at: 24 Oct. 2022.

73 SUN, C-Yu *et al.* From particle attachment to space-filling coral skeletons. **Proceedings of the National Academy of Sciences**, v. 117, n. 48, p. 30159–30170, Dec. 2020. DOI: 10.1073/pnas.2012025117.

74 MALIK, A. *et al.* Molecular and skeletal fingerprints of scleractinian coral biomineralization: from the sea surface to mesophotic depths. **Acta Biomaterialia**, v. 120, p. 263–276, Jan. 2021. ISSN 1742-7061. DOI: 10.1016/j.actbio.2020.01.010.

75 NOGUEIRA, M. M.; NEVES, E.; JOHNSSON, R. Effects of habitat structure on the epifaunal community in Mussismilia corals: does coral morphology influence the richness and abundance of associated crustacean fauna? **Helgoland Marine Research**, v. 69, n. 2, p. 221–229, June 2015. ISSN 1438-387X, 1438-3888. DOI: 10.1007/s10152-015-0431-x.

76 NOGUEIRA, J. M. M. Fauna living in colonies of Mussismilia hispida (Verrill) (Cnidaria:

Scleractinia) in four South-eastern Brazil islands. **Brazilian Archives of Biology and Technology**, v. 46, p. 421–432, June 2003. ISSN 1516-8913, 1678-4324. DOI: 10.1590/S1516-89132003000300014.

77 GARRIDO, C. **Dicionário de zoologia e sistemática dos invertebrados:** portugês, espanhol, inglês, alemão. São Paulo: EDUSP, 2019. 592 p. ISBN 978-85-314-1694-1.

78 ADDAMO, A. M.; MILLER, K. J.; HÄUSSERMANN, V.; TAVIANI, M.; MACHORDOM, A. Global-scale genetic structure of a cosmopolitan cold-water coral species. **Aquatic Conservation:** marine and freshwater ecosystems, v. 31, n. 1, p. 1–14, 2021. ISSN 1099-0755. DOI: 10.1002/aqc.3421.

79 KITAHARA, M. Species richness and distribution of azooxanthellate Scleractinia in Brazil. **Bulletin of Marine Science**, v. 81, p. 497–518, Nov. 2007.

80 NEULINGER, S. C.; JÄRNEGREN, J.; LUDVIGSEN, M.; LOCHTE, K.; DULLO, W-C. Phenotype-specific bacterial communities in the cold-water coral lophelia pertusa (scleractinia) and their implications for the coral's nutrition, health, and distribution. **Applied and Environmental Microbiology**, Dec. 2008. DOI: 10.1128/AEM.01777-08. Available from: https://journals.asm.org/doi/epdf/10.1128/AEM.01777-08. Accessible at: 26 Sept. 2022.

81 GERSTEIN, A. S. **Molecular biology problem solver:** a laboratory guide. New York: Wiley, 2001. 575 p. ISBN 978-0-471-37972-0.

82 XIE, S. S.; VASYLKIV, O.; TOK, A. I. Y. Highly ordered nano-scale structure in nacre of green-lipped mussel Perna canaliculus. **CrystEngComm**, v. 18, n. 39, p. 7501–7505, 2016. ISSN 1466-8033. DOI: 10.1039/C6CE01223J.

83 MCCUISTION, E. R. **The camel of time:** radiocarbon dating ther lower Pecos Canyonlands. Texas: Texas State University, 2019. 255 p.

84 **INTERPRETING Dates, Radiocarbon Dating Understood**. Available from: https://www.texasbeyondhistory.net/radiocarbon/interpreting.html#anchor-calibrateseveral. Accessible at: 27 Oct. 2022.

85 TOBY, B. H.; VON DREELE, R. B. *GSAS-II* : the genesis of a modern open-source all-purpose crystallography software package. **Journal of Applied Crystallography**, v. 46, n. 2, p. 544–549, Apr. 2013. ISSN 0021-8898. DOI: 10.1107/S0021889813003531.

86 ENGEL, A. S.; STERN, L. A.; BENNETT, P. C. Microbial contributions to cave formation: new insights into sulfuric acid speleogenesis. **Geology**, v. 32, n. 5, p. 369–372, May 2004. ISSN 0091-7613. DOI: 10.1130/G20288.1.

87 GHOSH, W.; DAM, B. Biochemistry and molecular biology of lithotrophic sulfur oxidation by taxonomically and ecologically diverse bacteria and archaea. **FEMS Microbiology Reviews**, v. 33, n. 6, p. 999–1043, Nov. 2009. ISSN 0168-6445. DOI: 10.1111/j.1574-6976.2009.00187. x.

88 GIBBARD, P. L.; HEAD, M. J. Chapter 30 - the quaternary period. *In*: GRADSTEIN, F. M.; OGG, J. G.; SCHMITZ, M. D.; OGG, G. M. (ed.). **Geologic time scale 2020**. Amsterdam: Elsevier, Jan. 2020. p. 1217–1255. ISBN 978-0-12-824360-2. DOI 10.1016/B978-0-12-824360-2.00030-9. Available from: https://www.sciencedirect.com/science/article/pii/B9780128243602000309. Accessible at: 20 Dec. 2022.

89 WALSH, S-J.; BRADING, P.; SUGGETT, D. J.; SMITH, D. J. Working with nature to identify coral reefs with increased environmental tolerance. *In*: INTERNATIONAL CORAL REEF SYMPOSIUM, 12., 2012. Available from: https://repository.essex.ac.uk/10443/1/ICRS2012_9A_14-libre.pdf. Accessible at: 20 Dec. 2022.

90 BREEZE, H.; DAVIS, D. S.; BUTLER, M.; KOSTYLEV, V. Distribution and status of deep sea corals off Nova Scotia. **Ecology Action Centre**, n. Marine Issues Committee Special Publication Number 1, 1997.

91 LARCOM, E. A.; MCKEAN, D. L.; BROOKS, J. M.; FISHER, C. R. Growth rates, densities, and distribution of Lophelia pertusa on artificial structures in the Gulf of Mexico. **Deep Sea Research Part I:** oceanographic research papers, v. 85, p. 101–109, Mar. 2014. ISSN 0967-0637. DOI: 10.1016/j.dsr.2013.12.005.

92 MAIER, S. R.; BANNISTER, R. J.; OEVELEN, D. VAN; KUTTI, T. Seasonal controls on the diet, metabolic activity, tissue reserves and growth of the cold-water coral Lophelia pertusa. **Coral Reefs**, v. 39, n. 1, p. 173–187, Jan. 2020. ISSN 1432-0975. DOI: 10.1007/s00338-019-01886-6.

93 GASS, S. E.; ROBERTS, J. M. Growth and branching patterns of Lophelia pertusa (Scleractinia) from the North Sea. **Journal of the Marine Biological Association of the United Kingdom**, v. 91, n. 4, p. 831–835, June 2011. ISSN 1469-7769, 0025-3154. DOI: 10.1017/S002531541000055X.

94 PIRES, D. O.; SEABRA, N. A.; SILVA, J. V. C. Recifes de coral de profundidade: corais construtores e sua distribuição no Brasil. **Brazilian Journal of Aquatic Science and Technology**, v. 19, n. 3, p. 51–61, 2015. ISSN 1983-9057. DOI: 10.14210/bjast.v19n3.4704.

95 RRUFF DATABASE: Raman, X-ray, infrared, and chemistry. **Aragonite R080142**. Available from: https://rruff.info/Aragonite/R080142. Accessible at: 26 Oct. 2022.

96 STOLARSKI, J.; PRZENIOSŁO, R.; MAZUR, M.; BRUNELLI, M. High-resolution synchrotron radiation studies on natural and thermally annealed scleractinian coral biominerals. **Journal of Applied Crystallography**, v. 40, n. 1, p. 2–9, Feb. 2007. ISSN 0021-8898. DOI: 10.1107/S002188980604489X.

97 HOEKSEMA, B. W.; CAIRNS, S. **World List of Scleractinia:** galaxea fascicularis (linnaeus, 1767). Available from: https://www.marinespecies.org/aphia.php?p=taxdetails&id=207366. Accessible at: 2 May 2023.

98 EMBLEM, Å.; KARLSEN, B. O.; EVERTSEN, J.; JOHANSEN, S. D. Mitogenome rearrangement in the cold-water scleractinian coral Lophelia pertusa (Cnidaria, Anthozoa) involves a long-term evolving group I intron. **Molecular Phylogenetics and Evolution**, v. 61, n. 2, p. 495–503, Nov. 2011. ISSN 1055-7903. DOI: 10.1016/j.ympev.2011.07.012.